HEME-REGULATED eIF2α KINASE MODULATES HEPATIC FGF21 AND IS ACTIVATED BY PPARβ/δ DEFICIENCY

Mohammad Zarei[1,2,3], Emma Barroso[1,2,3], Rosana Leiva[1], Marta Barniol-Xicota[1], Eugènia Pujol[1], Carmen Escolano[1], Santiago Vázquez[1], Xavier Palomer[1,2,3], Virginia Pardo[2,4], Águeda González-Rodríguez[2,4], Ángela M. Valverde[2,4],Tania Quesada-López[3,5,6], Francesc Villarroya[3,5,6], Walter Wahli [7,8,9] and Manuel Vázquez-Carrera[1,2,3]

[1]Department of Pharmacology, Toxicology and Therapeutic Chemistry, Faculty of Pharmacy, University of Barcelona, Institute of Biomedicine of the University of Barcelona (IBUB), Barcelona, Spain, [2]Spanish Biomedical Research Center in Diabetes and Associated Metabolic Diseases (CIBERDEM)-Instituto de Salud Carlos III, [3]Pediatric Research Institute-Hospital Sant Joan de Déu' [4]Instituto de Investigaciones Biomédicas Alberto Sols (CSIC/UAM), Madrid, Spain,[5]Department of Biochemistry and Molecular Biology and IBUB, University of Barcelona, [6]Spanish Biomedical Research Center in Physiopathology of Obesity and Nutrition (CIBEROBN)-Instituto de Salud Carlos III, [7]Center for Integrative Genomics, University of Lausanne, Lausanne, Switzerland, [8]Lee Kong Chian School of Medicine, Nanyang Technological University, Singapore 308232, [9]INRA ToxAlim, UMR1331, Chemin de Tournefeuille, Toulouse Cedex, France

Running title: Heme-regulated eIF2α kinase modulates hepatic FGF21

Corresponding author: Manuel Vázquez-Carrera. Unitat de Farmacologia. Facultat de Farmàcia. Diagonal 643. E-08028 Barcelona. Spain. Phone (+34) 93 4024531. Fax (+34) 93 4035982

E-mail: mvazquezcarrera@ub.edu

Number of figures: 8

***Abbreviations*:** FGF21, fibroblast growth factor 21; NAFLD, non-alcoholic fatty liver disease; PPAR, peroxisome proliferator-activated receptor; PGC-1α, PPARγ co-activator 1α; ATF4, activating transcription factor 4; HRI, heme-regulated eIF2α kinase; eIF2α, eukaryotic translation initiation factor 2α; BTdCPU, 1-(benzo[*d*][1,2,3]thiadiazol-6-yl)-3-(3,4-dichlorophenyl)urea; BTCtFPU, 1-(benzo[*d*][1,2,3]thiadiazol-6-yl)-3-(4-chloro-3-(trifluoromethyl)phenyl)urea; Cpt-1a, carnitine palmitoyl-transferase 1 a; Hmgcs2, 3-hydroxy-3-methylglutaryl-CoA synthase 2; Hsd3b5, 3-β-hydroxysteroid dehydrogenase type 5; Mup1, major urinary protein 1; Acox, acyl-CoA oxidase; Mcad, medium chain acyl-CoA dehydrogenase; Chop, C/EBP homologous protein; Orp150, oxygen-regulated protein of 150 kDa; IRE1α, inositol-requiring enzyme 1α; XBP1, X box-binding protein 1; AMPK, AMP-activated protein kinase; SIRT1, sirtuin 1; NRF-1, nuclear respiratory factor 1; mtOXPHOS, mitochondrial oxidative phosphorylation; Alas1, delta-aminolevulinate synthase 1; HFD, high-fat diet.

Keywords: ATF4; ER stress; Tunicamycin; HFD; palmitate.

Conflict of interest: Authors declare no competing interests.

Abstract

Fibroblast growth factor 21 (FGF21), a peptide hormone with pleiotropic effects on carbohydrate and lipid metabolism, is considered a target for the treatment of diabetes. In this study, we investigated the role of Peroxisome Proliferator-Activated Receptor (PPAR)β/δ deficiency in hepatic FGF21 regulation. Increased *Fgf21* expression was observed in liver of PPARβ/δ-null mice and in mouse primary hepatocytes when this receptor was knocked down by small interfering RNA (siRNA). Increased *Fgf21* was associated with enhanced protein levels in the heme-regulated eukaryotic translation initiation factor 2α (eIF2α) kinase (HRI). This increase caused enhanced levels of phosphorylated eIF2α and activating transcription factor (ATF) 4, which is essential for *Fgf21*-induced expression. siRNA analysis demonstrated that HRI regulates *Fgf21* expression in primary hepatocytes. Enhanced *Fgf21* expression attenuated tunicamycin-induced endoplasmic reticulum stress, as demonstrated by using a neutralizing antibody against FGF21. Interestingly, increased *Fgf21* expression in mice fed a HFD or hepatocytes exposed to palmitate was accompanied by reduced PPARβ/δ and activation of the HRI-eIF2α-ATF4 pathway. Moreover, pharmacological activation of HRI increased *Fgf21* expression and reduced lipid-induced hepatic steatosis and glucose intolerance and these effects were not observed in *Fgf21*-null mice. Overall, these findings suggest that HRI is a potential target for regulating hepatic FGF21 levels.

Introduction

Fibroblast growth factor 21 (FGF21), a member of the FGF family, functions as a hormone with a wide range of endocrine and autocrine actions on carbohydrate and lipid metabolism (1) and is considered a novel therapeutic target for the treatment of non-alcoholic fatty liver disease (NAFLD), insulin resistance and type 2 diabetes mellitus (T2DM). Several studies in genetic and diet-induced models of obesity have demonstrated that FGF21 administration ameliorates a large number of metabolic parameters (2-5), including plasma glucose and triglycerides levels and hepatic steatosis. However, despite these beneficial effects of administered FGF21, serum FGF21 levels are paradoxically increased in animal models of obesity (6). Likewise, circulating FGF21 levels are also elevated in patients with obesity, hypertriglyceridemia, TDM2 or NAFLD (7-9).

The pleiotropic effects of FGF21 on target tissues, including adipose tissue, β-cells and liver (1,10,11), are mediated by its binding to FGF receptors in a β-klotho-dependent manner (12-14). β-klotho is almost exclusively expressed in liver, adipose tissue, and pancreas (14), which may explain why these specific tissues are the predominant sites of action of FGF21. Circulating FGF21 is liver-derived (15), and hepatic *FGF21* expression is upregulated, following extended periods of fasting, by Peroxisome Proliferator-Activated Receptor (PPAR)α, a nuclear receptor that induces the expression of numerous genes involved in mitochondrial fatty acid oxidation (16). In recent years, it has also been reported that FGF21 is regulated by additional transcription factors, including cyclic AMP response element-binding protein H (17) and retinoic acid receptor-related orphan receptor α (18). Moreover, hepatic FGF21 is also negatively regulated by the PPARγ co-activator 1α (PGC-1α) by modulating the heme-sensing nuclear receptor REV-ERBα, which acts as a transcriptional repressor through its binding to ROR response elements (RORE) (19). Impaired mitochondrial oxidative phosphorylation is also responsible for *Fgf21* induction by activating transcription factor 4 (ATF4). ATF4 is a transcriptional effector of the protein kinase R-

like ER kinase (PERK)-branch of the endoplasmic reticulum (ER) stress/unfolded protein response pathway, which is essential for *Fgf21*-induced expression (20). However, although it has been reported that circulating FGF21 is increased following treatment with PPARβ/δ agonists (21), little is known about the effects of PPARβ/δ on FGF21 regulation in liver. PPARβ/δ is a ligand-activated transcription factor involved in the regulation of glucose and lipid homeostasis (22), and it has been proposed as a therapeutic target for the treatment of metabolic syndrome (23). Thus, genetic manipulations of PPARβ/δ as well as it activation by agonists attenuates dyslipidemia and hyperglycemia, improves whole-body insulin sensitivity, and prevents diet-induced obesity (24). In this study, we examined the effects of PPARβ/δ deficiency on hepatic *Fgf21* expression. *Pparβ/δ*-null mice showed enhanced hepatic *Fgf21* expression, which appears to be dependent on a reduction in PGC-1α levels and the subsequent reduction in hemin levels that finally activates the heme-regulated eIF2α kinase (HRI). This kinase phosphorylates the eIF2α, which in turn increases ATF4 levels, resulting in enhanced *Fgf21* expression. Overall, our findings point to HRI as a new therapeutic target for regulating *Fgf21* expression and metabolic dysregulation.

Research Design and Methods

Reagents

N,N'-diarylureas, 1-(benzo[d][1,2,3]thiadiazol-6-yl)-3-(3,4-dichlorophenyl)urea (BTdCPU) or 1-(benzo[d][1,2,3]thiadiazol-6-yl)-3-(4-chloro-3-(trifluoromethyl)phenyl)urea (BTCtFPU), were synthesized as previously described (25) (see Supplementary Methods).

Mice and cell culture

Male *Pparβ/δ* knockout (*Pparβ/δ*$^{-/-}$) mice and their wild-type littermates (*Pparβ/δ*$^{+/+}$) with the same genetic background (C57BL/6X129/SV) (26) and an initial weight of 20-25 g were fed a standard diet.

Lipid-containing media were prepared by conjugation of palmitic acid with fatty acid-free bovine serum albumin, as previously described (27). Primary mouse hepatocytes were isolated from non-fasting male C57BL/6 mice (10–12 weeks old) by perfusion with collagenase as described elsewhere (28).

Male mice (Harlan Ibérica S.A., Barcelona, Spain) were randomly distributed into three experimental groups (n=8 each): standard diet, Western-type high-fat diet (HFD, 35% fat by weight, 58% Kcal from fat, Harlan Ibérica S.A.) plus one daily oral gavage of vehicle (0.5% w/v carboxymethylcellulose), and HFD plus one daily oral dose of 3 mg kg^{-1} day^{-1} of the PPARβ/δ agonist GW501516 dissolved in the vehicle (volume administered 1 ml Kg^{-1}). In a second study, male mice received one daily i.p. administration of DMSO (vehicle) or BTdCPU (70 mg kg^{-1} day^{-1}) for 7 days. In a third study, male mice were randomly distributed into three experimental groups (n=8 each): standard chow or HFD for three weeks. Mice fed standard chow and half of the mice fed the HFD received one daily i.p. administration of DMSO (vehicle) for the last week. The rest of the mice fed the HFD received one daily i.p. administration of BTdCPU (70 mg kg^{-1} day^{-1}) for the last week. In a fourth study, male knockout (*Fgf21*$^{-/-}$) mice [B6N;129S5-*Fgf21*^{tm1Lex}/Mmcd, obtained from the Mutant Mouse Regional Resource Centre (MMRRC)] and their wild-type littermates (*Fgf21*$^{+/+}$) were treated as described in the third study.

RNA preparation and quantitative RT-PCR

The relative levels of specific mRNAs were assessed by Real-Time RT-PCR, as previously described (27). Primer sequences used for Real-Time RT-PCR are displayed in Supplementary Table 1.

Immunoblotting

Western blot analyses were performed as previously indicated (27).

Heme Protein Content Quantification

Heme content in liver was quantified by measuring the oxidized version of this protein, hemin, using an enzymatic assay kit (Hemin Assay Kit) (Sigma-Aldrich).

Oil Red Staining

Lipid accumulation in hepatocytes was assessed by Oil Red O staining as previously reported (29).

Statistical Analyses

Results are expressed as means ± S.D. Significant differences were established by one-way ANOVA using the GraphPad Instat program (GraphPad Software V5.01) (GraphPad Software Inc., San Diego, CA). When significant variations were found by one-way ANOVA, the Tukey-Kramer multiple comparison post-test was performed. Differences were considered significant at $p<0.05$.

Results

Ppar$\beta/\delta^{-/-}$ mice show increased hepatic Fgf21 expression and plasma levels

PPAR$\beta/\delta^{-/-}$ mice displayed higher hepatic *Fgf21* mRNA levels than wild-type litter mates (3-fold induction, $p<0.001$) (Fig. 1A). Consistent with the fact that circulating FGF21 is liver-derived (15),

we found increased plasma FGF21 levels in *Pparβ/δ*-deficient mice (2.6-fold increase, p<0.001) (Fig. 1B) and reduced expression of one of the receptor and co-receptor pairs used by FGF21, *Fgfr1c* (49 % reduction, p<0.05) and β-*Klotho* (57 % reduction, p<0.001) (Fig. 1C). Carnitine palmitoyl-transferase 1 a (*Cpt-1a*), 3-hydroxy-3-methylglutaryl-CoA synthase 2 (*Hmgcs2*) (30), 3-β-hydroxysteroid dehydrogenase type 5 (*Hsd3b5*) (31) and major urinary protein 1 (*Mup1*) (31) are FGF21 responsive genes. In accordance with increased FGF21 plasma levels, hepatic expression of *Cpt-1a* and *Hmgcs2* was increased, whereas the expression of *Hsd3b5*, and the mRNA and protein levels of MUP1 were decreased in *Pparβ/δ*$^{-/-}$ mice (Fig. 1D, Supplementary Fig. 1A). In agreement with the reported observation of increased glucose uptake in adipocytes through enhanced Glut1 expression by FGF21 secreted by the liver (32), the expression of this glucose transporter was higher in white adipose tissue of *Pparβ/δ*$^{-/-}$ mice than in wild-type animals (Fig. 1E). In contrast to the liver, the expression of *Fgf21* in white adipose tissue was not significantly increased in *Pparβ/δ*-deficient mice (Fig. 1E), pointing to a tissue-specific effect. Since increased serum free fatty acids (FFA) (33) and glucose levels (34) are two important stimuli that upregulate *Fgf21* expression in liver, we measured their levels in serum of *Pparβ/δ*$^{-/-}$ and wild-type mice. No differences were observed in serum FFA and glucose levels (Supplementary Fig. 1B and C), suggesting that they were not involved in the reported increase in *Fgf21* expression. In addition, the expression levels of *Pparα* and its target genes *Acox* and *Mcad* were not significantly increased, rendering it unlikely that PPARα is involved in the increase in *Fgf21* expression in these mice (Supplementary Fig. 1D). *Pparβ/δ*-null mice did not present upregulation of *Chop*, *Orp150* or *Atf3* expression (Supplementary Fig. 1E) nor of phospho-IRE1α and BiP levels (Supplementary Figure 1F), suggesting that ER stress was not the stimulus responsible for the increase in *Fgf21* expression. Primary hepatocytes were transfected with either control siRNA or *Pparβ/δ* siRNA showed a significant reduction (71%, p<0.001) in this transcription factor

(Supplementary Fig. 1G) and a significant increase in *Fgf21* gene expression (Fig. 1F), confirming that downregulation of *Pparβ/δ* in hepatocytes raises *Fgf21* expression.

Since AMPK (35) and SIRT1 (36) stimulate *Fgf21* expression, we explored the levels of these proteins in *Pparβ/δ*$^{-/-}$ mice. No changes were observed either in phosphorylated or total AMPK protein levels in *Pparβ/δ*-deficient mice compared to wild-type animals, whereas in accordance with the reported regulation of SIRT1 by PPARβ/δ (37), the protein levels of SIRT1 were reduced in *Pparβ/δ*$^{-/-}$ mice (Fig. 2A). Next, we focused on PGC-1α, since this transcriptional co-activator negatively regulates hepatic levels of *Fgf21* (19). *Pparβ/δ*-null mice showed reduced nuclear PGC-1α protein levels compared to wild-type mice (Fig. 2B). Since the reduction in PGC-1α upregulates *Fgf21* mRNA levels by decreasing the expression of the transcriptional repressor *Rev-Erbα* (19), we measured its mRNA and protein levels. *Pparβ/δ*$^{-/-}$ mice exhibited lower *Rev-Erbα* expression and protein levels than wild-type mice (Fig. 2B and C), which is consistent with the upregulation of Rev-Erbα-repressed *Bmal1* in *Pparβ/δ*-null mice (Fig. 2C). Since PGC-1α stimulates the expression of the *Nrf-1* gene (38), its reduction was in accordance with the reduction in hepatic PGC-1α (Fig. 2B). mtOXPHOS is regulated by both PGC-1α (39) and REV-ERBα (40), and their decrease is consistent with the reduction observed in the protein levels of several members of the mtOXPHOS in the liver of *Pparβ/δ*$^{-/-}$ mice (Fig. 2D). It has been reported that impaired mtOXPHOS is responsible for FGF21 induction by activating the eIF2α-ATF4 pathway (20). Although this pathway is activated by ER stress, the increase in phosphorylated eIF2α and activation of its downstream ATF4 signaling pathway can occur independently of ER stress, since eIF2α can also be phosphorylated by other kinases, including HRI (41). Interestingly, HRI is activated by heme deprivation (42) and PGC-1α is an important regulator of heme in liver cells since it co-activates NRF-1 and other transcription factors that increase the expression of *Alas1*, the rate-limiting enzyme in heme biosynthesis. In addition, the repressive activity of REV-ERBα

on *Fgf21* expression is potentiated by binding of its ligand heme (19). Given that *Pparβ/δ*$^{-/-}$ mice exhibited reduced PGC-1α and NRF-1 protein levels, we assessed heme content levels by measuring the oxidized form of this protein, hemin. *Pparβ/δ*$^{-/-}$ mice showed reduced levels of hemin compared to wild-type mice (Fig. 2E) and increased HRI levels in *Pparβ/δ*$^{-/-}$ mice compared to wild-type littermates (Fig. 2F). In agreement with the increase in HRI, levels of the downstream proteins of this pathway, phospho-eIF2α and ATF4, were also upregulated (Fig. 2F).

In accordance with the findings observed in the liver of *Pparβ/δ*-deficient mice, siRNA knockdown of *Pparβ/δ* in primary hepatocytes led to enhanced protein levels of HRI, phospho-eIF2α, ATF4 and reduced levels of MUP1 (Fig. 3A). Transfection of primary hepatocytes with siRNA against *Hri* caused a significant reduction in hemin levels and in the expression of *Fgf21, Atf4* and *Chop.* The latter being a direct ATF4 transcriptional target (43) used as a marker of the activation of the eIF2α-ATF4 pathway following activation of HRI (25) (Fig. 3B-E). Likewise, the protein levels of phosphorylated eIF2α, ATF4 and CHOP were decreased, whereas the protein levels of MUP1 were increased (Fig. 3F), confirming through a genetic approach that HRI controls *Fgf21* expression in hepatocytes.

PPARβ/δ regulates ER stress through hepatic Fgf21 expression

Hepatic *Fgf21* expression increases in response to ER stressors in liver, where it seems to play an adaptive response to these stimuli (44). In fact, exogenous administration of FGF21 alleviates the tunicamycin-induced eIF2α-ATF4-CHOP pathway, whereas it shows an insignificant effect on the IRE1α-XBP1s pathway (44). We hypothesized that the increase in FGF21 levels in *Pparβ/δ*-deficient mice may protect the liver against ER stress, which is consistent with the fact that, in contrast to the liver, skeletal muscle of these mice showed increased expression of ER stress

markers (45). To test this, wild-type and *Pparβ/δ*$^{-/-}$ mice were treated with the ER stressor tunicamycin for 24 h. Wild-type mice treated with tunicamycin exhibited a 9-fold increase ($p<0.001$) in *Fgf21* expression and this increase was higher (approximately 21-fold induction, $p<0.001$ vs. tunicamycin-treated wild-type mice) in liver of *Pparβ/δ*$^{-/-}$ mice (Fig. 4A). A similar effect was observed in plasma FGF21 levels (Fig. 4B). The mRNA and protein levels of the ER stress marker BiP were higher in the liver of tunicamycin-treated *Pparβ/δ*-deficient mice compared with tunicamycin-treated wild-type mice, suggesting that ER stress is exacerbated in the former (Supplementary Fig. 2A and 4C) probably as the result in the increase in ER stress pathways, such as the IRE1α-XBP1s, which are not inhibited by FGF21. The higher levels of FGF21 in vehicle-treated *Pparβ/δ*$^{-/-}$ mice compared with vehicle-treated wild-type mice were accompanied by a reduction in phospho-eIF2α protein levels (Fig. 4C). This was especially marked in tunicamycin-treated *Pparβ/δ*$^{-/-}$ mice when compared with tunicamycin-treated wild-type mice (Fig. 4C), suggesting that the higher levels of FGF21 in *Pparβ/δ*$^{-/-}$ mice inhibited the phosphorylation of eIF2α, as previously described (44). To clearly demonstrate this, we used an FGF21 neutralizing antibody. In wild-type mice, treatment with the FGF21 neutralizing antibody for 14 h did not significantly affect eIF2α phosphorylation compared to IgG-treated mice (Supplementary Fig. 2B). In contrast, when *Pparβ/δ*$^{-/-}$ mice were treated with the FGF21 neutralizing antibody for the same amount of time, a significant increase was observed in phospho-eIF2α levels (Fig. 4D). *Pparβ/δ*$^{-/-}$ mice treated for 14 h with tunicamycin and IgG showed a reduction in the levels of phospho-eIF2α, suggesting that the additional increase in FGF21 levels caused by tunicamycin treatment was responsible for this effect. In line with this, injection of the FGF21 neutralizing antibody raised phospho-eIF2α levels (Fig. 4D). The protein levels of ATF4 also showed an increase following treatment with the FGF21 neutralizing antibody (Fig. 4D). Through its negative action on eIF2α and ATF4, FGF21 can activate a negative feedback loop that reduces *Fgf21* expression

(44). Consistently, administration of the FGF21 neutralizing antibody raised the mRNA levels of *Fgf21* (Fig. 4E). The increase in *BiP* and *Atf3* expression and BiP protein levels confirmed that tunicamycin treatment for 14 h resulted in ER stress (Supplementary Fig. 2C-E).

Next, we explored whether the described mechanisms also operated in human HepG2 cells. Treatment with *Pparβ/δ* siRNA led to a significant increase in phosphorylated eIF2α and ATF4 levels (Fig. 4F), confirming that *Pparβ/δ* deficiency activates the eIF2α-ATF4 pathway. In addition, in the presence of the FGF21 neutralizing antibody, the increase in phospho-eIF2α and especially in ATF4 was exacerbated compared with IgG-treated cells. We then examined the effects of the FGF21 neutralizing antibody on tunicamycin-treated cells. In these cells, the FGF21 neutralizing antibody increased the levels of phosho-eIF2α and ATF4 protein levels compared with IgG-treated cells (Fig. 4F). Overall, these findings confirm that an increase in FGF21 levels in *Pparβ/δ*$^{-/-}$ mice prevents an increase in the eIF2α-ATF4 pathway, alleviating part of the ER stress process in liver.

PPARβ/δ activation prevents the increase in the HRI kinase-eIF2α-ATF4 pathway caused by a HFD in liver

Interestingly, exposure to a HFD increases *Fgf21* expression (11), and we have previously reported that exposure to HFD reduces hepatic mRNA levels of *Pgc-1α* (46). This suggests that exposure to a HFD might activate the HRI-eIF2α-ATF4 pathway, contributing to an increase in hepatic *Fgf21* expression. In mice exposed to a HFD for 3 weeks in the presence or absence of the PPARβ/δ activator GW501516 we observed that the HFD increased hepatic *Fgf21* expression (8-fold increase, $P<0.05$), whereas this increase was prevented by GW501516 (Fig. 5A). Consistent with the changes in *Fgf21* expression, feeding a HFD reduced MUP1 protein levels, whereas the PPARβ/δ agonist prevented the decrease caused by the HFD (Fig. 5B). No change was observed in

the protein levels of the ER stress marker BiP (Supplementary Fig. 3A), rendering it unlikely that ER stress might be responsible for the increase in *Fgf21* expression caused by a HFD. Interestingly, the HFD strongly reduced the protein levels of PPARβ/δ, PGC-1α and REV-ERBα, whereas ATF4 protein levels were increased (Fig. 5C). In contrast, these changes were abolished in mice fed the HFD and treated with GW501516. Furthermore, the reduction in PPARβ/δ, PGC-1α and REV-ERBα was accompanied by a reduction in hemin levels (Supplementary Fig. 3B) and an increase in HRI levels in mice fed the HFD, whereas this increase was blunted following drug treatment (Supplementary Fig. 3B and Fig. 5D). To confirm whether FAs were the HFD component responsible for the changes observed in the *in vivo* study, we exposed human Huh-7 hepatocytes to the SFA palmitate. Cells incubated with palmitate showed a huge increase in *FGF21* and *ATF4* expression (Fig. 5E). Palmitate also elicited a reduction in PPARβ/δ, PGC-1α and REV-ERBα and a subsequent increase in HRI, phospho-eIF2α and ATF4 protein levels (Fig. 5F). These findings suggest that by reducing PPARβ/δ and PGC-1α, SFA lead to activation of the HRI-eIF2α-ATF4 pathway and a subsequent increase in *FGF21* expression.

HRI is a pharmacological target to modulate hepatic Fgf21 expression

Given that HRI regulates *FGF21*, we next explored its suitability as a pharmacological target to modulate hepatic *FGF21* expression. For this purpose we used two N,N'-diarylureas, BTdCPU and BTCtFPU, which are HRI activators, thereby causing the phosphorylation of eIF2α and the increased expression of the transcription factor *ATF4* (25). Exposure of human Huh-7 hepatocytes to either 10 μM BTdCPU or BTCtFPU for 24 h strongly increased *Fgf21* and *Atf4* mRNA levels (Fig. 6A and B). The increase in the expression of *CHOP* (Fig. 6C), a direct ATF4 transcriptional target (43), confirmed that this pathway was activated by the N,N'-diaylureas. These compounds did not increase PPARα, nor its target genes, nor *BiP* mRNA (Supplementary Fig. 4A-D), nor BiP

protein levels (Fig. 6D), suggesting that these mechanisms were not involved in *Fgf21* upregulation. In line with the reported activation of HRI by these N,N'-diarylurea compounds, we observed increased protein levels of phospho-eIF2α and ATF4, especially following treatment with BTdCPU (Fig. 6D). Treatment of mice with BTdCPU for one week also increased hepatic *Fgf21* expression (Fig. 6E), without changes in BiP protein levels, whereas phospho-eIF2α and ATF4 were increased (Fig. 6F). Moreover, consistent with the increased expression of *Fgf21*, *Glut1* mRNA levels were higher in the white adipose tissue of mice treated with BTdCPU (Fig. 6G).

Next, we explored the effects of BTdCPU on human Huh-7 hepatocytes exposed to the SFA palmitate. Cells exposed to this FA showed increased *FGF21, ATF4* and CHOP mRNA levels and when cells were co-incubated with the FA and BTdCPU, a significant higher increase was observed in the expression of these three genes (Fig. 7A). Interestingly, when HuH7 cells were exposed to palmitate, a high accumulation of triglycerides was observed in the cells, as demonstrated by Oil Red O (ORO) staining, but this accumulation was prevented in the presence of the BTdCPU compound, and this effect was attenuated in the presence of the FGF21 neutralizing antibody (Fig. 7B and Supplementary Fig. 5A). Similar effects were observed in mouse Hepa-1c1c7 hepatocytes (Supplementary Fig. 5B). Likewise, this compound partially restored the reduction in insulin-stimulated Akt phosphorylation caused by palmitate (Fig. 7C and Supplementary Fig. 5C), showing that this drug treatment prevents SFA-induced attenuation of the insulin signaling pathway. Next, we examined the effects of the BTdCPU compound in mice fed a HFD. Of note, BTdCPU administration prevented the glucose intolerance caused by HFD feeding (Fig. 7D), increased *Glut1* expression in white adipose tissue (Fig. 7E) and prevented hepatic steatosis, as demonstrated by ORO and eosin-hematoxylin staining and quantification of hepatic triglyceride levels (Fig. 7F and G). Drug treatment did not affect the expression of PPARα-target genes (Supplementary Fig. 5D and E), whereas the expression of the lipogenic gene fatty acid

synthase (*Fas*) and stearoyl-CoA desaturase 1 (*Scd1*) was reduced (Supplementary Figure 5F and G), which is consistent with the reported reduction of these genes by FGF21 (47).

To clearly demonstrate that the improvement in glucose tolerance and hepatic steatosis caused by the administration of the HRI activator in mice fed a HFD is dependent on FGF21 we used WT and *Fgf21*-null mice. The reduction in glucose intolerance observed in WT mice fed a HFD caused by administration of the HRI activator was completely abolished in *Fgf21*-null mice (Fig. 8A), suggesting that in the absence of FGF21 the effect of the HRI activator on glucose tolerance is lost. Similarly, the reduction in hepatic triglyceride accumulation in WT fed a HFD caused by BTdCPU administration was suppressed in *Fgf21*-null mice, as demonstrated by the analysis of the levels of triglyceride and the ORO and eosin-hematoxylin staining (Fig. 8B and C).

Discussion

FGF21 has emerged as an important regulator of glucose and lipid metabolism and hence is a promising agent for the treatment of obesity, NAFLD, insulin resistance and type 2 diabetes mellitus. Unraveling the mechanisms that regulate *Fgf21* expression in liver may provide pharmacological targets for modulating its expression to prevent metabolic diseases. In this study, we demonstrate that *Pparβ/δ*-null mice show enhanced hepatic *Fgf21* expression and circulating levels of this hormone. *Pparβ/δ* deficiency caused a reduction in transcriptional co-activator PGC-1α levels that resulted in a reduction in hemin levels and the subsequent activation of HRI and the eIF2α-ATF4 pathway, which is essential for *Fgf21*-induced expression (Fig. 8). Likewise, activation of this pathway could be an additional mechanism that can contribute to the increase in *Fgf21* expression under lipid overload conditions. Our findings revealed HRI as a regulator of *Fgf21* expression, and consistent with this, knockdown of *Hri* or its pharmacological activation regulates *Fgf21* expression in hepatocytes.

The finding that *Pparβ/δ* deficiency upregulates *Fgf21* expression in liver was unexpected since it has previously been reported that pharmacological activation of this nuclear receptor increases FGF21 levels (21). The latter is consistent with the discovery of two putative peroxisome proliferator response elements (PPRE) in the mouse and human *FGF21* promoters (48) and with the fact that both PPARα and PPARγ activators increase FGF21 levels in hepatocytes and adipocytes, respectively. However, genetically reduced PGC-1α, a transcriptional co-activator that controls the expression and activity of PPARs and is also regulated by these transcription factors, likewise results in increased FGF21 levels (19). In fact, it has been reported that reduced hepatic PGC-1α upregulates *Fgf21* expression by reducing REV-ERBα and the levels of its ligand heme. This alleviated the repressive activity of REV-ERBα on the *Fgf21* promoter leading to enhanced *Fgf21* expression. In the present study, we show that *Pparβ/δ* deficiency results in a reduction in PGC-1α levels that leads to a reduction in REV-ERBα and hemin, the oxidized form of heme, suggesting that this mechanism can also contribute to an increase in *Fgf21* expression in the liver of *Pparβ/δ*-null mice. In addition, our findings also provide a new biochemical pathway that can contribute to the enhanced expression of *Fgf21* in the liver of these mice. Indeed, the reduction in heme can increase HRI levels (43), which in turn can activate the eIF2α-ATF4 pathway, where the increase in ATF4 is one of the most important transcription factors that upregulate *Fgf21* expression. In fact, it has been reported that overexpression of ATF4 induces *Fgf21* expression (20), whereas knockdown of *Atf4* reduces basal and ER stress-induced *Fgf21* expression (49). Therefore, our findings indicate that *Pparβ/δ* deficiency in liver results in increased levels of ATF4 and a subsequent increase in *Fgf21* expression. The increase in ATF4 levels seems to be a crucial step in *Fgf21* upregulation, since this transcription factor is involved in the increase of this hormone in impaired mitochondrial OXPHOS induced by autophagy deficiency (20), ER stress

(49), metformin-induced inhibition of the mitochondrial respiratory chain (50) and now PPARβ/δ-PGC-1α deficiency, as shown by this study.

The eIF2α-ATF4 pathway is activated by ER stress leading to enhanced *Fgf21* expression, which in turn alleviates ER stress by suppressing this eIF2α-ATF4 pathway, as has been demonstrated by injection of recombinant FGF21 (44). By using a neutralizing antibody against FGF21, we have confirmed that this negative feedback is also activated by FGF21.

Interestingly, the reduction in PPARβ/δ and PGC-1α following exposure to a HFD might also contribute to increased *Fgf21* expression. In fact, livers of mice exposed to a HFD or hepatocytes exposed to the saturated fatty acid palmitate showed reduced PPARβ/δ and PGC-1α levels, resulting in an increase in the levels of HRI and subsequent activation of the eIF2α-ATF4 pathway. These findings suggest that activation of this pathway could also contribute to the increase in FGF21 in those conditions associated with fat overfeeding, such as obesity, type 2 diabetes mellitus, or NAFLD, which show increased levels of this hormone (7-9). In contrast, activation of PPARβ/δ under conditions of lipid overload recovers PGC-1α levels and attenuates the eIF2α-ATF4 pathway, restoring *Fgf21* expression.

The regulation of FGF21 by the eIF2α kinase HRI provides a target for regulation of the levels of this hormone to prevent or treat metabolic diseases, including NAFLD, insulin resistance, and diabetes. *N,N'*-diarylureas are activators of HRI that cause phosphorylation of eIF2α developed as anticancer drugs (25). Here we show that these drugs can increase *Fgf21* expression in hepatocytes and that their administration to mice fed a HFD prevents the accumulation of triglycerides in liver and improves glucose intolerance. This is consistent with the fact that liver-specific *Fgf21* knockout mice fed a HFD displayed glucose intolerance and increased hepatic lipid accumulation

(15). Moreover, we have demonstrated that the improvement in glucose tolerance and hepatic steatosis caused by the HRI activator BTdCPU in mice fed a HFD is dependent on FGF21, since it was not observed in *Fgf21*-null mice.

In summary, on the basis of our findings we propose that *Pparβ/δ* deficiency results in a reduction in hepatic PGC-1α and hemin levels that in turn increase HRI levels, leading to activation of the eIF2α-ATF4 pathway and a subsequent increase in *Fgf21* expression. Moreover, pharmacological activation of the eIF2α kinase HRI increases *Fgf21* expression and treatment with a drug that activates HRI prevents glucose intolerance and hepatic triglyceride accumulation in mice fed a HFD. These findings point to HRI as a target for the treatment of metabolic diseases by modulating FGF21 levels.

ACKNOWLEDGMENTS- R. L. thanks the Spanish Ministry of Education for a PhD Grant (FPU program). M.B.-X. thanks the Institute of Biomedicine of the University de Barcelona (IBUB) for a PhD grant. M.Z. thanks Dr. Bijan Almassian.

Financial Support. This study was partly supported by funds from the Spanish Ministry of the Economy and Competitiveness (SAF2012-30708 and SAF2015-64146-R to MVC, SAF2014-55725 to FV and SAF2015-65267-R to AMV) and European Union ERDF funds. CIBER de Diabetes y Enfermedades Metabólicas Asociadas (CIBERDEM) and CIBER Fisiopatologia de la Obesidad y Nutrición (CIBERobn) are Carlos III Health Institute project. WW is supported by Start-Up Grants from the Lee Kong Chian School of Medicine, Nanyang Technological University,

Singapore and by the Région Midi-Pyrénées, France and TQL is supported by a CONACyT (National Council for Science and Technology in Mexico) Ph.D. scholarship.

Author's contribution: MZ, EB, XP, TQL,VP, AGR, AMV, and MVC performed the experiments; RL, MBX, EP, CE, and SV synthesized the compounds; WW and FV analyzed the data and revised the results; MZ and MVC designed the experiments and revised the results; MVC was primarily responsible for writing the manuscript. All authors contributed to manuscript editing and approval.

References

1. Potthoff MJ, Kliewer SA, Mangelsdorf DJ. Endocrine fibroblast growth factors 15/19 and 21: from feast to famine. Genes Dev 2012;26:312-324.
2. Kharitonenkov A, Shiyanova TL, Koester A, Ford AM, Micanovic R, Galbreath EJ, Sandusky GE, Hammond LJ, Moyers JS, Owens RA, Gromada J, Brozinick JT, Hawkins ED, Wroblewski VJ, Li DS, Mehrbod F, Jaskunas SR, Shanafelt AB. FGF-21 as a novel metabolic regulator. J Clin Invest 2005;115:1627-1635.
3. Xu J, Lloyd DJ, Hale C, Stanislaus S, Chen M, Sivits G, Vonderfecht S, Hecht R, Li YS, Lindberg RA, Chen JL, Jung DY, Zhang Z, Ko HJ, Kim JK, Véniant MM. Fibroblast growth factor 21 reverses hepatic steatosis, increases energy expenditure, and improves insulin sensitivity in diet-induced obese mice. Diabetes 2009;58:250-259.
4. Xu J, Stanislaus S, Chinookoswong N, Lau YY, Hager T, Patel J, Ge H, Weiszmann J, Lu SC, Graham M, Busby J, Hecht R, Li YS, Li Y, Lindberg R, Véniant MM. Acute glucose-lowering and insulin-sensitizing action of FGF21 in insulin-resistant mouse models--association with liver and adipose tissue effects. Am J Physiol Endocrinol Metab 2009;297:E1105-1114.
5. Coskun T, Bina HA, Schneider MA, Dunbar JD, Hu CC, Chen Y, Moller DE, Kharitonenkov A. Fibroblast growth factor 21 corrects obesity in mice. Endocrinology 2008;149:6018-6027.
6. Badman MK, Kennedy AR, Adams AC, Pissios P, Maratos-Flier E. A very low carbohydrate ketogenic diet improves glucose tolerance in ob/ob mice independently of weight loss. Am J Physiol Endocrinol Metab 2009;297:E1197-1204.
7. Zhang X, Yeung DC, Karpisek M, Stejskal D, Zhou ZG, Liu F, Wong RL, Chow WS, Tso AW, Lam KS, Xu A. Serum FGF21 levels are increased in obesity and are independently associated with the metabolic syndrome in humans. Diabetes 2008;57:1246-1253.
8. Chavez AO, Molina-Carrion M, Abdul-Ghani MA, Folli F, Defronzo RA, Tripathy D. Circulating fibroblast growth factor-21 is elevated in impaired glucose tolerance and

type 2 diabetes and correlates with muscle and hepatic insulin resistance. Diabetes Care 2009;32:1542-1546.
9. Li H, Fang Q, Gao F, Fan J, Zhou J, Wang X, Zhang H, Pan X, Bao Y, Xiang K, Xu A, Jia W. Fibroblast growth factor 21 levels are increased in nonalcoholic fatty liver disease patients and are correlated with hepatic triglyceride. J Hepatol 2010;53:934-940.
10. Kharitonenkov A, Shiyanova TL, Koester A, Ford AM, Micanovic R, Galbreath EJ, Sandusky GE, Hammond LJ, Moyers JS, Owens RA, Gromada J, Brozinick JT, Hawkins ED, Wroblewski VJ, Li DS, Mehrbod F, Jaskunas SR, Shanafelt AB. FGF-21 as a novel metabolic regulator. J Clin Invest 2005;115:1627-1635.
11. Kharitonenkov A, Larsen P. FGF21 reloaded: challenges of a rapidly growing field. Trends Endocrinol Metab 2011;22:81-86.
12. Kharitonenkov A, Dunbar JD, Bina HA, Bright S, Moyers JS, Zhang C, Ding L, Micanovic R, Mehrbod SF, Knierman MD, Hale JE, Coskun T, Shanafelt AB. FGF-21/FGF-21 receptor interaction and activation is determined by betaKlotho. J Cell Physiol 2008;215:1-7.
13. Ogawa Y1, Kurosu H, Yamamoto M, Nandi A, Rosenblatt KP, Goetz R, Eliseenkova AV, Mohammadi M, Kuro-o M. BetaKlotho is required for metabolic activity of fibroblast growth factor 21. Proc Natl Acad Sci U S A 2007;104:7432-7437.
14. Suzuki M, Uehara Y, Motomura-Matsuzaka K, Oki J, Koyama Y, Kimura M, Asada M, Komi-Kuramochi A, Oka S, Imamura T. betaKlotho is required for fibroblast growth factor (FGF) 21 signaling through FGF receptor (FGFR) 1c and FGFR3c. Mol Endocrinol 2008;22:1006-1014.
15. Markan KR, Naber MC, Ameka MK, Anderegg MD, Mangelsdorf DJ, Kliewer SA, Mohammadi M, Potthoff MJ. Circulating FGF21 is liver derived and enhances glucose uptake during refeeding and overfeeding. Diabetes 2014;63:4057-4063.
16. Lefebvre P, Chinetti G, Fruchart JC, Staels B. Sorting out the roles of PPAR alpha in energy metabolism and vascular homeostasis. J Clin Invest 2006;116:571-580.
17. Kim H, Mendez R, Zheng Z, Chang L, Cai J, Zhang R, Zhang K. Liver-enriched transcription factor CREBH interacts with peroxisome proliferator-activated receptor α to regulate metabolic hormone FGF21. Endocrinology 2014;155:769-782.
18. Wang Y, Solt LA, Burris TP. Regulation of FGF21 expression and secretion by retinoic acid receptor-related orphan receptor alpha. J Biol Chem 2010;285:15668-15673.
19. Estall JL, Ruas JL, Choi CS, Laznik D, Badman M, Maratos-Flier E, Shulman GI, Spiegelman BM. PGC-1alpha negatively regulates hepatic FGF21 expression by modulating the heme/Rev-Erb(alpha) axis. Proc Natl Acad Sci U S A 2009;106:22510-22515.
20. Kim KH, Jeong YT, Oh H, Kim SH, Cho JM, Kim YN, Kim SS, Kim do H, Hur KY, Kim HK, Ko T, Han J, Kim HL, Kim J, Back SH, Komatsu M, Chen H, Chan DC, Konishi M, Itoh N, Choi CS, Lee MS. Autophagy deficiency leads to protection from obesity and insulin resistance by inducing Fgf21 as a mitokine. Nat Med 2013;19:83-92.
21. Christodoulides C, Dyson P, Sprecher D, Tsintzas K, Karpe F. Circulating fibroblast growth factor 21 is induced by peroxisome proliferator-activated receptor agonists but not ketosis in man. J Clin Endocrinol Metab 2009;94:3594-3601.
22. Evans RM1, Barish GD, Wang YX. PPARs and the complex journey to obesity. Nat Med 2004;10:355-361.

23. Salvadó L, Serrano-Marco L, Barroso E, Palomer X, Vázquez-Carrera M. Targeting PPARβ/δ for the treatment of type 2 diabetes mellitus. Expert Opin Ther Targets 2012;16:209-223.
24. Giordano Attianese GM, Desvergne B. Integrative and systemic approaches for evaluating PPARβ/δ (PPARD) function. Nucl Recept Signal 2015;13:e001.
25. Chen T, Ozel D, Qiao Y, Harbinski F, Chen L, Denoyelle S, He X, Zvereva N, Supko JG, Chorev M, Halperin JA, Aktas BH. Chemical genetics identify eIF2α kinase heme-regulated inhibitor as an anticancer target. Nat Chem Biol 2011;7:610-616.
26. Nadra K, Anghel SI, Joye E, Tan NS, Basu-Modak S, Trono D, Wahli W, Desvergne B. Differentiation of trophoblast giant cells and their metabolic functions are dependent on peroxisome proliferator-activated receptor beta/delta. Mol Cell Biol 2006;26:3266-3281.
27. Salvadó L, Coll T, Gómez-Foix AM, Salmerón E, Barroso E, Palomer X, Vázquez-Carrera M. Oleate prevents saturated-fatty-acid-induced ER stress, inflammation and insulin resistance in skeletal muscle cells through an AMPK-dependent mechanism. Diabetologia 2013;56:1372-1382.
28. Benveniste R, Danoff TM, Ilekis J, Craig HR. Epidermal growth factor receptor numbers in male and female mouse primary hepatocyte cultures. Cell Biochem Funct 1988;6:231-235.
29. Koopman R, Schaart G, Hesselink MKC. Optimisation of oil red O staining permits combination with immunofluorescence and automated quantification of lipids. Histochem Cell Biol 2001;116:63–68.
30. Li H, Gao Z, Zhang J, Ye X, Xu A, Ye J, Jia W. Sodium butyrate stimulates expression of fibroblast growth factor 21 in liver by inhibition of histone deacetylase 3. Diabetes 2012;61:797-806.
31. Inagaki T, Lin VY, Goetz R, Mohammadi M, Mangelsdorf DJ, Kliewer SA. Inhibition of growth hormone signaling by the fasting-induced hormone FGF21. Cell Metab 2008;8:77-83.
32. Ge X, Chen C, Hui X, Wang Y, Lam KS, Xu A. Fibroblast growth factor 21 induces glucose transporter-1 expression through activation of the serum response factor/Ets-like protein-1 in adipocytes. J Biol Chem 2011;286:34533-34541.
33. Badman MK, Pissios P, Kennedy AR, Koukos G, Flier JS, Maratos-Flier E. Hepatic fibroblast growth factor 21 is regulated by PPARalpha and is a key mediator of hepatic lipid metabolism in ketotic states. Cell Metab 2007;5:426-437.
34. Iizuka K, Takeda J, Horikawa Y. Glucose induces FGF21 mRNA expression through ChREBP activation in rat hepatocytes. FEBS Lett 2009;583:2882-2886.
35. Nygaard EB1, Vienberg SG, Ørskov C, Hansen HS, Andersen B. Metformin stimulates FGF21 expression in primary hepatocytes. Exp Diabetes Res 2012;2012:465282.
36. Li Y, Wong K, Giles A, Jiang J, Lee JW, Adams AC, Kharitonenkov A, Yang Q, Gao B, Guarente L, Zang M. Hepatic SIRT1 attenuates hepatic steatosis and controls energy balance in mice by inducing fibroblast growth factor 21. Gastroenterology 2014;146:539-549.
37. Okazaki M, Iwasaki Y, Nishiyama M, Taguchi T, Tsugita M, Nakayama S, Kambayashi M, Hashimoto K, Terada Y. PPARbeta/delta regulates the human SIRT1 gene transcription via Sp1. Endocr J 2010;57:403-413.
38. Wu Z, Puigserver P, Andersson U, Zhang C, Adelmant G, Mootha V, Troy A, Cinti S, Lowell B, Scarpulla RC, Spiegelman BM. Mechanisms controlling mitochondrial

biogenesis and respiration through the thermogenic coactivator PGC-1. Cell. 1999;98:115-124.
39. St-Pierre J, Lin J, Krauss S, Tarr PT, Yang R, Newgard CB, Spiegelman BM. Bioenergetic analysis of peroxisome proliferator-activated receptor gamma coactivators 1alpha and 1beta (PGC-1alpha and PGC-1beta) in muscle cells. J Biol Chem 2003;278:26597-26603.
40. Woldt E, Sebti Y, Solt LA, Duhem C, Lancel S, Eeckhoute J, Hesselink MK, Paquet C, Delhaye S, Shin Y, Kamenecka TM, Schaart G, Lefebvre P, Nevière R, Burris TP, Schrauwen P, Staels B, Duez H. Rev-erb-α modulates skeletal muscle oxidative capacity by regulating mitochondrial biogenesis and autophagy. Nat Med 2013;19:1039-1046.
41. Ron D, Walter P. Signal integration in the endoplasmic reticulum unfolded protein response. Nat Rev Mol Cell Biol 2007;8:519-529.
42. Chen JJ. Regulation of protein synthesis by the heme-regulated eIF2alpha kinase: relevance to anemias. Blood 2007;109:2693-2699.
43. Lu PD, Harding HP, Ron D. Translation reinitiation at alternative open reading frames regulates gene expression in an integrated stress response. J Cell Biol 2004;167:27-33.
44. Jiang S, Yan C, Fang QC, Shao ML, Zhang YL, Liu Y, Deng YP, Shan B, Liu JQ, Li HT, Yang L, Zhou J, Dai Z, Liu Y, Jia WP. Fibroblast growth factor 21 is regulated by the IRE1α-XBP1 branch of the unfolded protein response and counteracts endoplasmic reticulum stress-induced hepatic steatosis. J Biol Chem 2014;289:29751-29765.
45. Salvadó L, Barroso E, Gómez-Foix AM, Palomer X, Michalik L, Wahli W, Vázquez-Carrera M. PPARβ/δ prevents endoplasmic reticulum stress-associated inflammation and insulin resistance in skeletal muscle cells through an AMPK-dependent mechanism. Diabetologia 2014;57:2126-2135.
46. Barroso E, Rodríguez-Calvo R, Serrano-Marco L, Astudillo AM, Balsinde J, Palomer X, Vázquez-Carrera M. The PPARβ/δ activator GW501516 prevents the down-regulation of AMPK caused by a high-fat diet in liver and amplifies the PGC-1α-Lipin 1-PPARα pathway leading to increased fatty acid oxidation. Endocrinology 2011;152:1848-1859.
47. Zhang Y, Lei T, Huang JF, et al. The link between fibroblast grothw factor 21 and sterol regulatory element binding protein 1c during lipogenesis in hepatocytes. Mol Cell Endocrinol 2011;342:41-47.
48. Lundåsen T, Hunt MC, Nilsson LM, Sanyal S, Angelin B, Alexson SE, Rudling M. PPARalpha is a key regulator of hepatic FGF21. Biochem Biophys Res Commun 2007;360:437-40.
49. Kim SH, Kim KH, Kim HK, Kim MJ, Back SH, Konishi M, Itoh N, Lee MS. Fibroblast growth factor 21 participates in adaptation to endoplasmic reticulum stress and attenuates obesity-induced hepatic metabolic stress. Diabetologia 2015;58:809-818.
50. Kim KH, Jeong YT, Kim SH, Jung HS, Park KS, Lee HY, Lee MS. Metformin-induced inhibition of the mitochondrial respiratory chain increases FGF21 expression via ATF4 activation. Biochem Biophys Res Commun 2013;440:76-81.

Figure legends

Fig. 1. ***Fgf21*** **expression is increased in liver of** ***Pparβ/δ*****-null mice and in primary hepatocytes following knockdown of** ***Pparβ/δ*****.** Liver and epididymal white adipose tissue from male wild-type and *Pparβ/δ*-null mice were used (n=6 per group). A, assessment by quantitative real-time RT-PCR of hepatic *Fgf21*. B, serum FGF21 levels. Data are presented as the mean ± S.D. (n=6 per group) relative to the wild-type mice. C, mRNA abundance of hepatic *Fgfr1c* and *β-klotho*. D, mRNA abundance of hepatic *L-Cpt-1*, *Hmgcs2*, *Hsd3b5* and *Mup1*. E, mRNA abundance of epididymal white adipose tissue *Fgf21* and *Glut1*. F, *Fgf21* mRNA abundance in primary hepatocytes transfected with control siRNA or *Pparβ/δ* siRNA for 24 h. mRNA levels are presented as the mean ± S.D. (n=6 per group). ***p<0.001 and *p<0.05 vs. wild-type mice or control siRNA.

Fig. 2. ***Pparβ/δ*** **deficiency decreases PGC-1α and hemin levels and activates the HRI-eIF2α-ATF4 pathway.** A, liver cell lysates and nuclear extracts from male wild-type and *Pparβ/δ*-null mice were assayed for Western blot analysis with antibodies against total and phospho-AMPK and SIRT1. Data are presented as the mean ± S.D. (n=6 per group) relative to the wild-type mice. B, nuclear extracts were assayed by Western blot analysis with antibodies against PGC-1α, REV-ERBα and NRF-1. C, *Rev-Erbα* and *Bmal1* mRNA levels in liver from wild-type and *Pparβ/δ*-null mice. Data are presented as the mean ± S.D. (n=6 per group) relative to the wild-type mice. D, immunoblot analyses of mitochondrial OXPHOS proteins. E, liver hemin levels. Data are presented as the mean ± S.D. (n=6 per group) relative to the wild-type mice. F, immunoblot analyses of HRI, total and phospho-eIF2α and ATF4. **p<0.01 and *p<0.05 *vs.* wild-type mice.

Fig. 3. ***Hri*** **knockdown in primary hepatocytes reduces** ***Fgf21*** **expression.** A, primary hepatocytes were transfected with control or *Pparβ/δ* siRNA for 24 hours and the protein levels of HRI, phospho and total eIF2α, ATF4 and MUP1 analyzed by immunoblotting. B, hemin levels. *Fgf21* (C), *Atf3* (D) and *Chop* (E) mRNA abundance in primary hepatocytes transfected with control or *Hri* siRNA for 24 hours. F, immunoblot analyses of HRI, total and phospho-eIF2α, ATF4, CHOP and MUP1 in primary hepatocytes transfected with control siRNA or *Hri* siRNA for 24 hours. Data are presented as the mean ± S.D. (n=6 per group). ***p<0.001 and *p<0.05 *vs.* control siRNA.

Fig. 4. **Increased** ***Fgf21*** **expression in liver of** ***Pparβ/δ*****-null mice alleviates ER stress.** Male wild-type and *Pparβ/δ*-null mice were treated for 24 h through i.p. injection with DMSO (vehicle) or tunicamycin (Tunic) (3 mg kg^{-1} body weight) and the mRNA abundance of hepatic *Fgf21* (A) and serum levels of FGF21 (B) were determined. Data are presented as the mean ± S.D. (n=6 per group). C, immunoblot analyses of BiP, total and phospho-eIF2α. Data are presented as the mean ± S.D. (n=6 per group). ***p<0.001, **p<0.01 and *p<0.05 *vs.* wild-type animals treated with DMSO (vehicle). $^{###}$p<0.001, $^{##}$p<0.01 and $^{#}$p<0.05 *vs.* wild-type animals treated with tunicamycin. †††p<0.001 and ††p<0.01 *vs. Pparβ/δ*-null mice treated with DMSO (vehicle). D, male wild-type and *Pparβ/δ*-null mice at 12 weeks of age were injected intraperitoneally with IgG (9 μg/mouse) or a neutralizing antibody (Ab) (9 μg/mouse) against FGF21 together with DMSO or tunicamycin (Tunic) (3 mg kg^{-1} body weight). Mice were sacrificed at 14 h after treatment. Immunoblot analyses of total and phospho-eIF2α and ATF4 were performed in liver lysates. Data are presented as the mean ± S.D. (n=4 per group). E, mRNA abundance of hepatic *Fgf21*.

***p<0.001, **p<0.01 and *p<0.05 *vs. Pparβ/δ*-null mice treated with IgG and DMSO. ###p<0.001, ##p<0.01 and #p<0.05 *vs. Pparβ/δ*-null mice treated with neutralizing antibody against FGF21 and DMSO. ††p<0.01 and †p<0.05 *vs. Pparβ/δ*-null mice treated with IgG and tunicamycin. F, HepG2 cells transfected with control siRNA or PPARβ/δ siRNA were co-incubated with tunicamycin (2 μg/ml) and IgG (3 μg/ml) or a neutralizing antibody (Ab) (3 μg/ml) against FGF21 for 24 hours. Immunoblot analyses of total and phospho-eIF2α and ATF4 were performed in cell lysates. ***p<0.001, **p<0.01 and *p<0.05 *vs.* control siRNA. #p<0.05 *vs.* PPARβ/δ siRNA. †p<0.05 *vs.* cells transfected with *PPARβ/δ* siRNA incubated with IgG. &&&p<0.001 and &p<0.05 *vs.* cells transfected with *PPARβ/δ* siRNA co-incubated with IgG and tunicamycin.

Fig. 5. **The increase in hepatic *Fgf21* expression caused by feeding a high-fat diet (HFD) is associated with a reduction in PPARβ/δ and subsequent activation of the HRI-eIF2α-ATF4 pathway.** Male mice were fed a standard chow or HFD with or without GW501516 (3 mg kg^{-1} day^{-1}). Animals were sacrificed after three weeks of treatment. A, assessment by quantitative real-time RT-PCR of hepatic *Fgf21*. Data are presented as the mean ± S.D. (n=6 per group) relative to the control (CT) group. Immunoblot analyses of MUP1 (B), PPARβ/δ, PGC-1α, REV-ERBα and ATF4 (C) and HRI (D). Data are presented as the mean ± S.D. (n=6 per group). ***p<0.001, **p<0.01 and *p<0.05 vs. CT group. ###p<0.001, ##p<0.01 and #p<0.05 *vs.* mice fed a HFD. E, Huh-7 hepatocytes were incubated for 16 h in the absence (Control, CT) or in the presence of 0.5 mmol/L palmitate (Pal). mRNA abundance of *FGF21*and *ATF4.* Data are presented as the mean ± S.D. (n=6 per group). F, immunoblot analyses of PPARβ/δ, PGC-1α, REV-ERBα, HRI, total and phospho-eIF2α and ATF4. Data are presented as the mean ± S.D. (n=5 per group). ***p<0.001 and *p<0.05 vs. CT group.

Fig. 6. **HRI activators increase *FGF21* expression in hepatocytes.** Huh-7 hepatocytes were incubated for 16 h in the absence (Control, CT) or in the presence of 10 μmol/L of either BTdCPU or BTCtFPU. mRNA abundance of *FGF21* (A), ATF4 (B) and CHOP (C). D, immunoblot analyses of BiP, total and phospho-eIF2α and ATF4. *Fgf21* mRNA abundance (E) and immunoblot analyses (F) of BiP total and phospho-eIF2α and ATF4 in the livers of mice treated with DMSO (vehicle) or BTdCPU (70 mg kg^{-1} day^{-1}) for 7 days. G, *Glut1* mRNA abundance in white adipose tissue of mice treated with DMSO (vehicle) or BTdCPU (70 mg kg^{-1} day^{-1}) for 7 days. Data are presented as the mean ± S.D. (n=5 per group). ***p<0.001, **p<0.01 and *p<0.05 vs. CT group.

Fig. 7. **HRI activation prevents HFD-induced glucose intolerance and hepatic steatosis.** Huh-7 cells were incubated for 24 h with BSA (Control, CT), 0.75 mmol/L palmitate conjugated with BSA or 0.75 mmol/L palmitate plus 10 μmol/L BTdCPU. A, mRNA levels of *FGF21, ATF4* and *CHOP*. Data are presented as the mean ± S.D. (n=5 per group). ***p<0.001 and *p<0.05 vs. CT group. $^{###}$p<0.001 and $^{#}$p<0.05 *vs.* palmitate-exposed cells. B, Oil Red O staining of Huh-7 cells. Huh-7 cells were incubated for 24 h with BSA (Control, CT), 0.75 mmol/L palmitate conjugated with BSA, 0.75 mmol/L palmitate plus 10 μmol/L BTdCPU and IgG (3 μg/ml) or 0.75 mmol/L palmitate plus 10 μmol/L BTdCPU and a FGF21 neutralizing antibody (3 μg/ml). C, immunoblot analyses of total and phosphorylated Akt. When indicated, cells were incubated with 100 nmol/L insulin for the last 10 min. Data are presented as the mean ± S.D. (n=4 per group). ***p<0.001 *vs.* control cells not exposed to insulin. $^{###}$p<0.001 *vs.* insulin-stimulated control cells. †††p<0.001 *vs.* insulin-stimulated cells incubated with palmitate. D, glucose tolerance test and area under the curve (AUC) of mice fed a standard chow, a HFD for three weeks or a HFD for three weeks plus BTdCPU during the last week. Mice fed a standard chow and half of the mice fed the HFD received one daily i.p. administration of DMSO (vehicle) for the last week. The rest of the mice

fed the HFD received one daily i.p. administration of BTdCPU (70 mg kg^{-1} day^{-1}) for the last week. Data are presented as the mean ± S.D. (n=6 per group). E, *Glut1* mRNA abundance in the white adipose tissue. F, eosin-hematoxylin and Oil Red O staining of livers. G, liver triglyceride levels. **p<0.01 and *p<0.05 *vs.* mice fed a standard diet (CT). $^{###}$p<0.001 and $^{#}$p<0.05 *vs.* mice fed a HFD.

Fig. 8. The beneficial effects of HRI pharmacological activation in glucose intolerance and hepatic steatosis are dependent on FGF21. A, glucose tolerance test and area under the curve (AUC) of WT and *Fgf21*-null mice fed a standard chow, a HFD for three weeks or a HFD for three weeks plus BTdCPU during the last week. Mice fed a standard chow and half of the mice fed the HFD received one daily i.p. administration of DMSO (vehicle) for the last week. The rest of the mice fed the HFD received one daily i.p. administration of BTdCPU (70 mg kg-1 day-1) for the last week. Data are presented as the mean ± S.D. (n=5 per group). B, liver triglyceride levels. C, eosin-hematoxylin and Oil Red O staining of livers. ***p<0.001 and *p<0.05 vs. WT mice fed a standard diet (CT). $^{##}$p<0.01 and $^{#}$p<0.05 vs. mice fed a HFD. ††p<0.01 and †p<0.05 vs. *Fgf21*-null mice fed a standard diet. D, Schematic representation of the potential role of *Pparβ/δ* deficiency in the regulation of hepatic *Fgf21* expression via activation of the HRI-eIF2α-ATF4 pathway. *Pparβ/δ* deficiency and overconsumption of HFD can result in the activation of this pathway, contributing to the increase in *Fgf21* expression observed under these conditions.

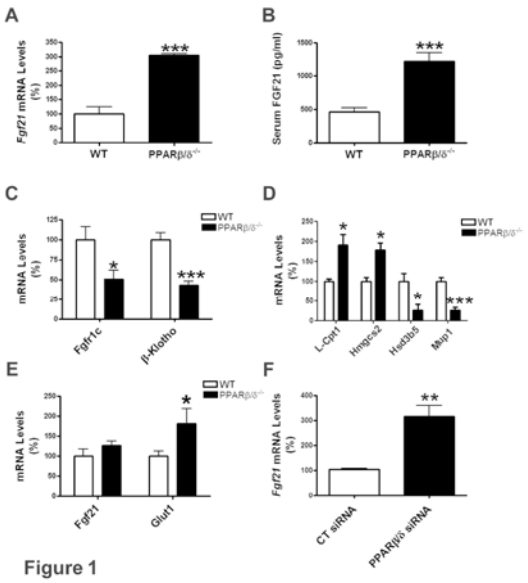

Figure 1

Figure 1

209x297mm (300 x 300 DPI)

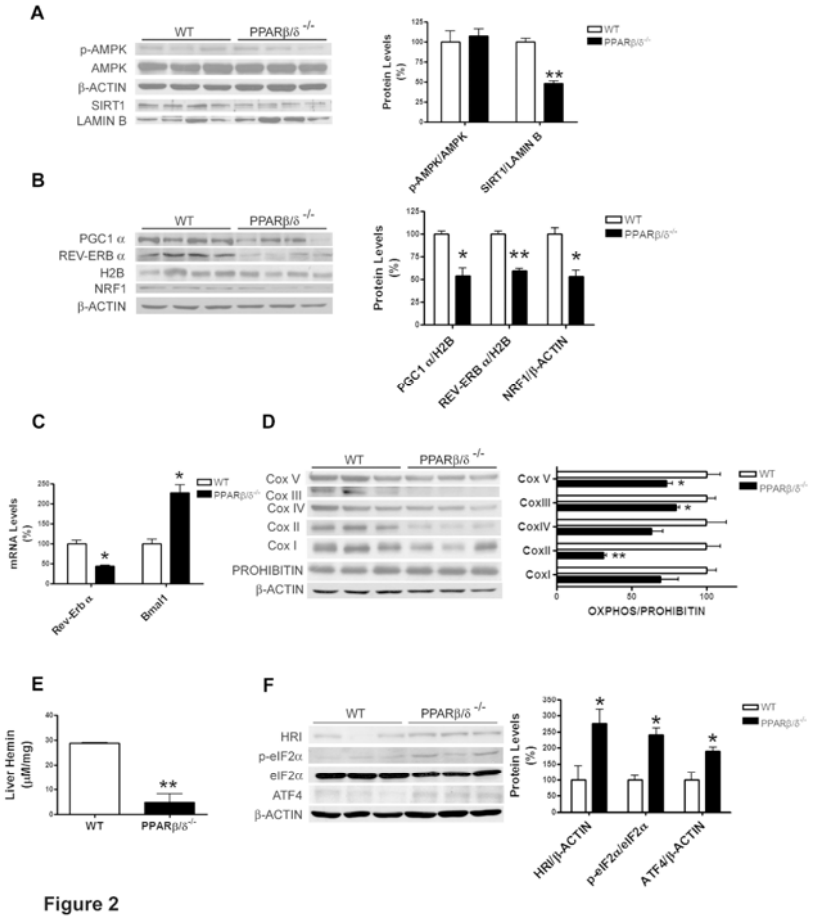

Figure 2

Figure 2

209x297mm (300 x 300 DPI)

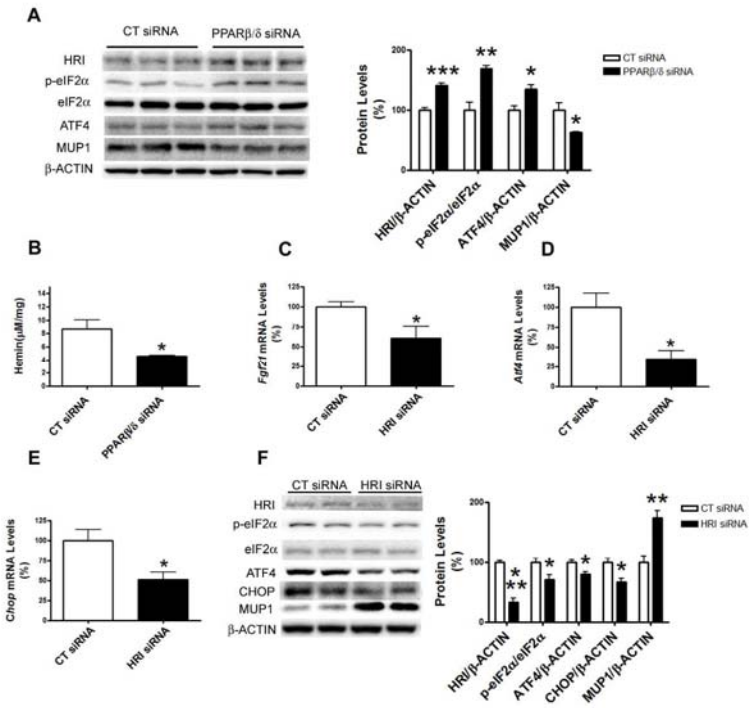

Figure 3

Figure 3

209x297mm (300 x 300 DPI)

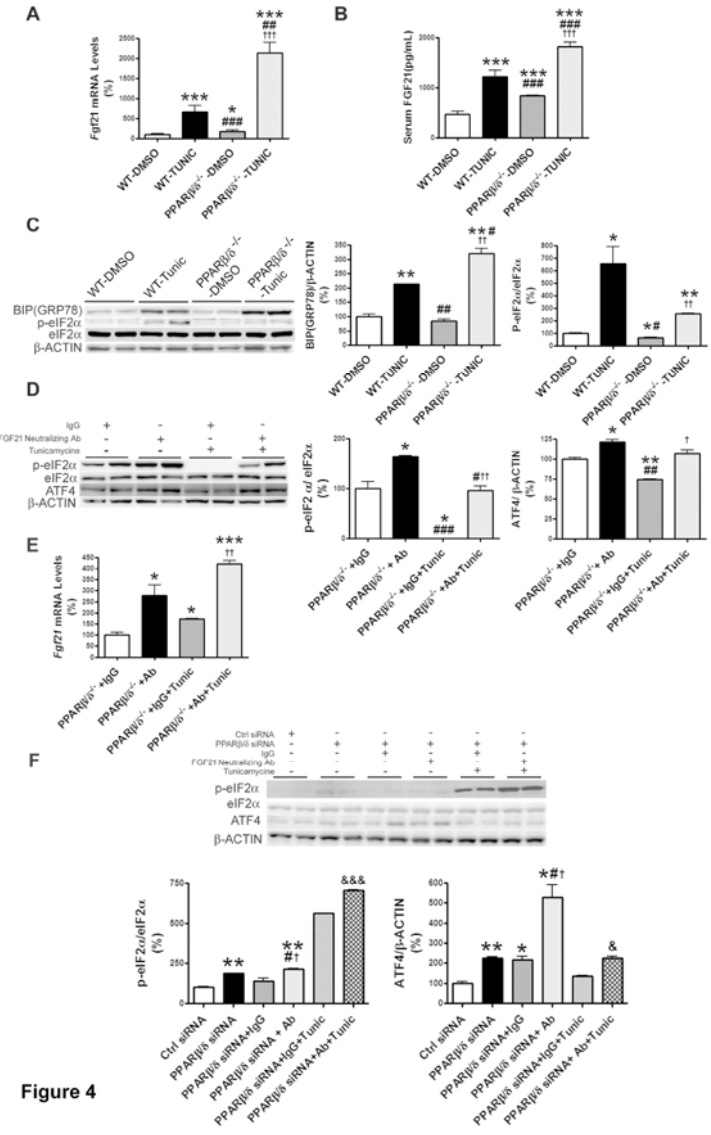

Figure 4

Figure 4

209x297mm (300 x 300 DPI)

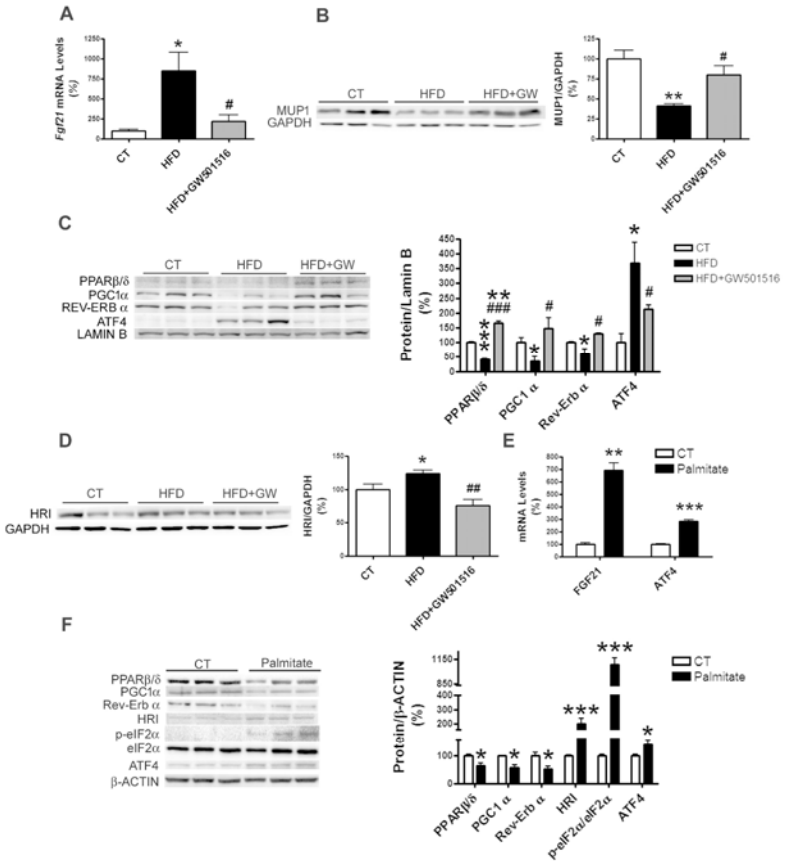

Figure 5

Figure 5

209x297mm (300 x 300 DPI)

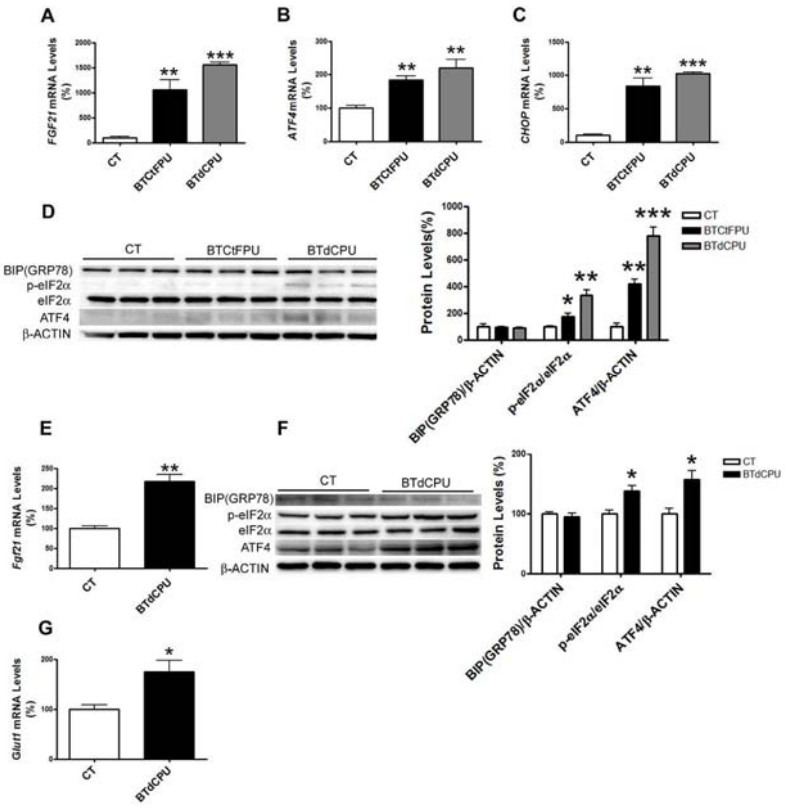

Figure 6

Figure 6

209x297mm (300 x 300 DPI)

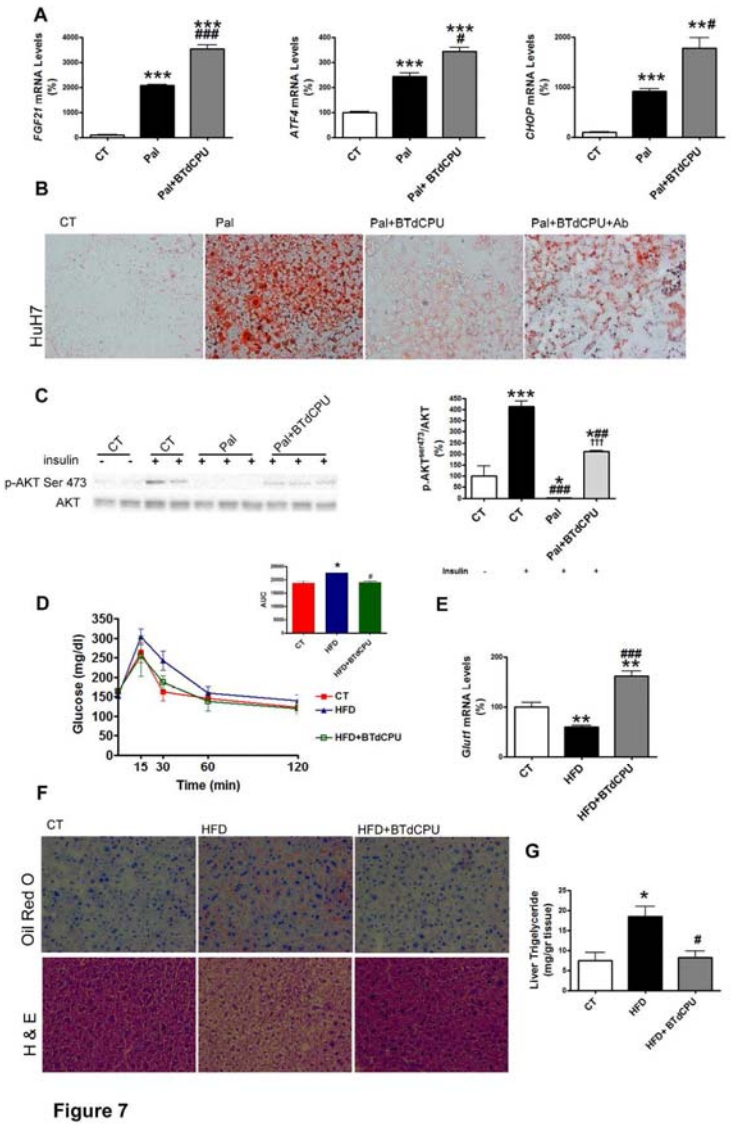

Figure 7

Figure 7

209x297mm (300 x 300 DPI)

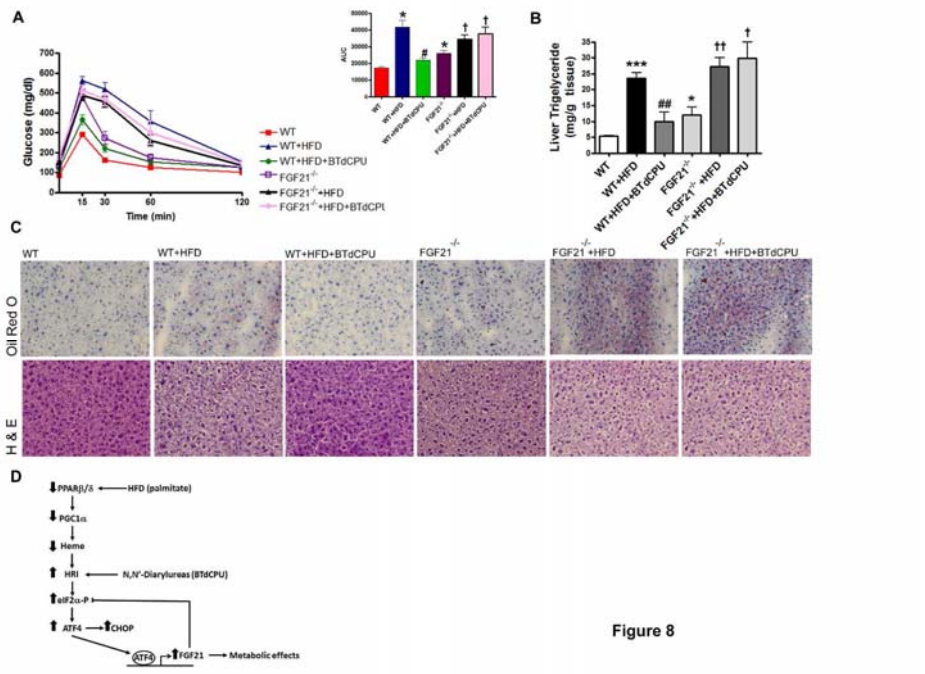

Figure 8

297x209mm (300 x 300 DPI)

Supplementary Materials

The research complied with the Guide for the Care and Use of Laboratory Animals published by the US National Institutes of Health (NIH Publication No. 85-23, revised 1996). All procedures were approved by the University of Barcelona Bioethics Committee, as stated in Law 5/21 July 1995 passed by the Generalitat de Catalunya.

Reagents

Control and HRI siRNA were purchased from Santa Cruz (Dallas, TX) and PPARβ/δ siRNA from GE Dharmacon (Lafayette, CO). Human and mouse FGF21 neutralizing antibodies were purchased from Antibody and Immunoassays Services (Hong Kong, China).

Plasma FGF21 was measured using a rat/mouse FGF21 ELISA kit (Millipore, Bedford, MA). Serum glucose (Bayer Iberia, Sant Joan Despí, Spain), triglyceride (Sigma) and free fatty acid (FFA) (Wako, Japan) levels were measured using commercial kits.

Cell culture

Human HepG2 and Huh-7 and mouse Hepa1c1c7 cells were purchased from the ATCC and cultured in DMEM supplemented with 10% serum, at 37°C/5% CO2. siRNA transfections were performed with Lipofectamine 2000 (Life Technologies).

Synthesis of N,N'-diarylureas

Step 1. (2-Amino-5-nitrophenyl) disulphide 2

15 g (83.4 mmol) 6-nitrobenzothiazole 1 was suspended in abs. ethanol (300 mL). Hydrazine hydrate (30 mL, 600 mmol) was added and the mixture was refluxed for 2 h, converting from a yellow mixture to a dark red solution. The reaction was cooled to 30 °C and 50% hydrogen peroxide (16.2 mL) was added in small portions, maintaining the temperature with an ice water bath. On completion, the red color disappeared and a yellow precipitate formed. The suspension was stirred for 1 h, the precipitate was

collected, washed with water and diethyl ether, and dried to give 11.71 g of product 2. Yield: 83.5%. 1H-NMR (400 MHz, DMSO) δ: 6.85 (d, J = 9.2 Hz, 2 H, 3-H), 7.21 (b. s., 4 H, NH2), 7.51 (d, J = 2.6 Hz, 2 H, 6-H), 7.99 (dd, J = 9.2 Hz, J' = 2.6 Hz, 2 H, 4-H).

Step 2. 6-Nitro-1,2,3-benzothiadiazole 3

11.68 g (34.5 mmol) (2-amino-5-nitrophenyl) disulphide 2 was dissolved in concentrated sulfuric acid (96 mL), chilled to 0 °C, and 5.45 g (86.3 mmol) sodium nitrite was added in small portions, while the temperature was kept under 10 °C. The reaction was allowed to warm to room temperature and stirred for 18 h. The reaction mixture was poured into a mixture of 650 g ice and water (65 mL), stirred for 1 h, and the pale brown precipitate was collected, then washed with water and diethyl ether. The crude product was taken up in dichloromethane (1 x 300 mL), filtered, and the filtrate was treated with a small amount of charcoal (1 g), filtered, and evaporated to give 5.29 g of a brown solid. Yield: 42.3% NMR: 90%. Column chromatography on alumina (Hexane 95%/Ethyl acetate 5% mixture) gave product 3 as a yellow solid (3.45 g). 1H-NMR (400 MHz, CDCl3) δ: 8.51 (dd, J = 9.2 Hz, J' = 2.0 Hz, 1 H, 5-H), 8.80 (d, J = 9.2 Hz, 1 H, 4-H), 9.04 (d, J = 2.0, 1 H, 7-H). 13C-NMR (100.5 MHz, CDCl3) δ: 115.7 (CH, C7), 122.0 (CH, C5), 124.8 (CH, C4), 141.1 (C, C3a), 147.7 (C, C7a), 159.5 (C, C6).

Step 3. 6-Amino-1,2,3-thiadiazole 4

2 g (11.0 mmol) 6-nitro-1,2,3-benzothiadiazole 3 was added to a solution of 10.6 g tin (II) chloride in concentrated hydrochloric acid (16 mL) at 55 °C, using a water bath to maintain that temperature. The reaction mixture was heated to 70 °C for 10 min, then cooled to 4 °C and let stand for 18 h. The crystalline precipitate was collected and washed with ice cold water. The solid was dissolved in water (40 mL) and 10 N sodium hydroxide (10 mL) was added followed by ethyl acetate (30 mL) and the mixture was stirred for 15 min. The layers were separated; the aqueous layer was extracted with, then ethyl acetate (1 x 30 mL, 1 x 20 mL). The organic layers were combined, washed with saturated brine (1 x 20 mL), water (1 x 20 mL) and evaporated to give 0.97 g of product 4. Yield: 58%. 1H-NMR (400 MHz, CDCl3) δ: 4.20 (b. s., 2 H, NH2), 6.92 (dd, J = 9.2 Hz, J' = 2.4 Hz, 1 H, 5-H), 7.13 (d, J = 2.4 Hz, 1 H, 7-H), 8.34 (d, J = 9.2, 1 H, 4-H). 13C-NMR (100.5 MHz, CDCl3) δ: 100.4 (CH, C7), 117.0 (CH, C5), 124.5 (CH, C4), 143.8 (C, C3a), 148.1 (C, C7a), 152.9 (C, C6).

1.44 g (7.9 mmol) 6-nitro-1,2,3-benzothiadiazole 3 was added to a solution of 7.6 g tin (II) chloride in concentrated hydrochloric acid (12 mL) at 55 °C, using a water bath to maintain that temperature. The reaction mixture was heated to 70 °C for 10 min, then cooled to 4 °C and let stand for 18 h. The crystalline precipitate was dissolved in water (20 mL) and 10 N sodium hydroxide (5 mL) was added followed by ethyl acetate (20 mL) and the mixture was stirred for 15 min. The layers were separated; the aqueous layer was extracted with, then ethyl acetate (1 x 20 mL, 1 x 10 mL). The organic layers were combined, washed with saturated brine (1 x 20 mL), water (1 x 20 mL) and evaporated to give 0.84 g of product 4. Yield: 70%

Step 4a. 1-(1,2,3-Benzothiadiazol-6-yl)-3-(4-chloro-3-(trifluoromethyl)phenyl)urea 5
0.5 g (3.31 mmol) 6-Amino-1,2,3-thiadiazole 4, and 0.81 g (3.64 mmol) 4-chloro-3-(trifluoromethyl)phenyl isocyanate were dissolved in tetrahydrofuran (13 mL), and stirred at room temperature for 2.5 h; a white precipitate formed. IR (ATR) ν: 659, 679, 720, 749, 782, 812, 840, 863, 875, 910, 949, 1026, 1130, 1173, 1220, 1249, 1268, 1321, 1352, 1403, 1469, 1484, 1545, 1573, 1708, 3094, 3132, 3266, 3302, 3339. 1H-NMR (400 MHz, CDCl3) δ: 7.63-7.67 (c. s., 2 H, 5'-H, 6'-H), 7.69 (dd, J = 9.2 Hz, J' = 2.0 Hz, 1 H, 5-H), 8.17 (d, J = 2.0 Hz, 1 H, 2'-H), 8.59 (d, J = 9.2 Hz, 1 H, 4-H), 8.63 (d, J = 2.0, 1 H, 7-H), 9.38 (b. s., 1 H, NH), 9.52 (b. s., 1 H, NH). 13C-NMR (100.5 MHz, CDCl3) δ: 106.8 (CH, C7), 117.0 (q, J = 6.1 Hz, CH, C2'), 119.8 (CH, C5), 122.76 (q, J = 273.2 Hz, C, CF3), 122.83 (q, J = 2.0 Hz, C, C4'), 123.3 (b. s., CH, C5'), 123.6 (CH, C4), 126.7 (q, J = 31.0 Hz, C, C3'), 132.0 (CH, C6'), 138.9 (C, C1'), 140.8 (C, C3a), 142.2 (C, C7a), 152.2 (C, C6), 153.8 (C, CO). Calcd for C14H8ClF3N4OS · 2/3 H20: C 43.70, H 2.45, N 14.56. Found: C 43.75, H 2.43, N 14.60.

Step 4b. 1-(1,2,3-Benzothiadiazol-6-yl)-3-(3,4-dichlorophenyl)urea 6
0.5 g (3.31 mmol) 6-Amino-1,2,3-thiadiazole 4, and 0.68 g (3.64 mmol) 3,4dichlorophenyl isocyanate were dissolved in tetrahydrofuran (13 mL), and stirred at room temperature for 2.5 h; a white precipitate formed. Methanol (0.3 mL) was added and the mixture was stirred for 15 min, cooled to 0 °C in an ice-water bath, stirred for 30 min, and the precipitate was collected and washed with ice cold tetrahydrofuran to give 0.71 g of product 6 (68% yield), mp 267 – 269 °C (dec). IR (ATR) ν: 685, 731, 746, 805, 856, 881, 910, 1026, 1060, 1129, 1220, 1265, 1304, 1351, 1385, 1417, 1455,

1467, 1531, 1567, 1673, 3098, 3171, 3306. 1H-NMR (400 MHz, CDCl3) δ: 7.38 (dd, J = 9.2 Hz, J' = 2.4 Hz, 1 H, 6'-H), 7.55 (d, J = 9.2 Hz, 1 H, 5'-H), 7.69 (dd, J = 9.2 Hz, 1 H, J' = 2.0 Hz, 1 H, 5-H), 7.91 (d, J = 2.4 Hz, 1 H, 2'-H), 8.56-8.60 (c. s., 2 H, 4-H, 7-H), 9.20 (b. s., 1 H, NH), 9.47 (b. s., 1 H, NH). 13C-NMR (100.5 MHz, CDCl3) δ: 106.7 (CH, C7), 118.6 (CH, C6'), 119.6 (CH, C2'), 119.7 (CH, C5), 123.58 (C, C4), 123.64 (C, C4'), 130.6 (CH, C6'), 131.1 (C, C3'), 731, 746,139.5 (C, C1'), 140.8 (C, C3a), 142.2 (C, C7a), 152.1 (C, C6), 153.8 (C, CO). Calcd for C13H8Cl2N4OS: C 46.03, H 2.38, N 16.52. Found: C 45.89, H 2.36, N 16.10.

Supplementary Figure legends

Supplementary Figure 1. A, liver cell lysates from male wild-type and PPAR*β/δ*-null mice were assayed for Western-blot analysis with antibodies against MUP-1 and *β*-actin. Data are presented as the mean ± S.D. (n=6 per group) relative to the wild-type mice. Serum free fatty acids (FFA) (B) and glucose (C) levels in wild-type and PPAR*β/δ*-null mice. D, mRNA levels of hepatic *Pparα*, *Acox1* and *Mcad*. E, mRNA abundance of *Chop*, *Orp150* and *Atf3*. F, immunoblot analyses of total and phospho-IRE1. Data are presented as the mean ± S.D. (n=6 per group). G, *PPARβ/δ* mRNA abundance in primary hepatocytes transfected with control siRNA or PPAR*β/δ* siRNA for 24 h. $^{***}p<0.001$ and $^{**}p<0.01$ vs. wild-type mice.

Supplementary Figure 2. A, Male wild-type and PPAR*β/δ*-null mice at 12 weeks of age were treated for 24 h through intraperitoneal injection with DMSO (vehicle) or tunicamycin (Tunic) (3 mg kg^{-1} body weight) and the mRNA abundance of hepatic *BiP* was determined. B, male wild-type mice were injected intraperitoneally with IgG or a neutralizing antibody (Ab) against FGF21. Immunoblot analyses of total and phospho-eIF2*α*. Data are presented as the mean ± S.D. (n=6 per group). Male wild-type and PPAR*β/δ*-null mice were injected intraperitoneally with IgG or a neutralizing antibody (Ab) against FGF21 together with DMSO or tunicamycin (Tunic) (3 mg kg^{-1} body weight). Mice were sacrificed at 14 h after treatment. mRNA abundance of hepatic *BiP* (C) and *Atf3* (D). Data are presented as the mean ± S.D. (n=6 per group). E, immunoblot analyses of hepatic BiP. Data are presented as the mean ± S.D. (n=4 per group). $^{***}p<0.001$, $^{**}p<0.01$ and $^{*}p<0.05$ *vs.* PPAR*β/δ*-

null mice treated with IgG and DMSO. $^{###}p<0.001$, $^{##}p<0.01$ and $^{#}p<0.05$ *vs.* PPARβ/δ-null mice treated with neutralizing antibody against FGF21 and DMSO. $^{†††}p<0.001$ *vs.* PPARβ/δ-null mice treated with IgG and tunicamycine.

Supplementary Figure 3. Male mice were fed a standard chow or HFD with or without GW501516 (3 mg kg^{-1} day^{-1}). Animals were sacrificed after three weeks of treatment. A, Immunoblot analyses of BiP. B, hemin levels. Data are presented as the mean ± S.D. (n=6 per group).

Supplementary Figure 4. Huh-7 hepatocytes were incubated for 24 h in the absence (Control, CT) or in the presence of 10 µmol/L of either BTdCPU or BTCtFPU. mRNA abundance of PPARα (A), ACOX (B), MCAD (C) and BiP (D Data are presented as the mean ± S.D. (n=5 per group).

Supplementary Figure 5. Oil Red O staining of Huh-7 (A) and Hepa1c1c7 (B) hepatocytes. Cells were incubated for 24 h with BSA (Control, CT), 0.75 mmol/L palmitate (Pal) conjugated with BSA, 0.75 mmol/L palmitate plus 10 µmol/L BTdCPU and IgG (3 μg/ml) or 0.75 mmol/L palmitate plus 10 µmol/L BTdCPU and a FGF21 neutralizing antibody (Ab) (3 μg/ml). C, immunoblot analyses of total and phosphorylated Akt at Thr^{308}. When indicated, cells were incubated with 100 nmol/L insulin for the last 10 min. Data are presented as the mean ± S.D. (n=4 per group). $^{***}p<0.001$ and $^{**}p<0.01$ vs. control cells not exposed to insulin. $^{###}p<0.001$ and $^{##}p<0.01$ vs. insulin-stimulated control cells. $^{†}p<0.05$ vs. insulin-stimulated cells incubated with palmitate. mRNA abundance of MCAD (D), ACOX (E), FAS (F) and SCD1 (G) in the livers of mice fed a standard chow, a HFD for three weeks or a HFD for three weeks plus BTdCPU during the last week. Mice fed a standard chow

and half of the mice fed the HFD received one daily i.p. administration of DMSO (vehicle) for the last week. The rest of the mice fed the HFD received one daily i.p. administration of BTdCPU (70 mg kg-1 day-1) for the last week. Data are presented as the mean ± S.D. (n=5 per group). $^{**}p<0.01$ and $^{*}p<0.05$ vs. mice fed a standard diet (CT). $^{\#}p<0.05$ vs. mice fed a HFD.

Supplementary Table 1. Primer sequences used for real-time RT- PCR

Gene	Primers	
mAprt	for	5'-CAGCGGCAAGATCGACTACA-3'
	rev	5'-AGCTAGGGAAGGGCCAAACA-3'
mAtf3	for	5'-CTGGAGATGTCAGTCACCAAGTCT-3'
	rev	5'-TTTCTCGCCGCCTCCTTT-3'
mAtf4	for	5'-AGCAAAACAAGACAGCAGCC-3'
	rev	5'-ACTCTCTTCTTCCCCCTTGC-3'
hATF4	for	5'-GCGGGCTCCTCCGAAT-3'
	rev	5'-ATCCTCCTTGCTGTTGTTGGA-3'
mAcox	for	5'-TCTGGAGATCACGGGCACTT-3'
	rev	5'-TTTCCAAGCCTCGAAGATGAG-3'
hACOX	for	5'-GGAAAAAAACTCGGGCAGAAC-3'
	rev	5'-TGGCGAGGAACTCTGACCTT-3'
mβ-Klotho	for	5`-TGGGGTCCCATTGGATAGAG-3`
	rev	5`-ACTCAGGGTAGTCGCCGTC-3`
mBip	for	5`-CAGATCTTCTCCACGGCTTC-3`
	rev	5`-GCAGGAGGAATTCCAGTCAG-3`
hBIP	for	5`-ACTATTGCTGGCCTAAATGTTATGAG-3`
	rev	5`-TTATCCAGGCCATAAGCAATAGC-3`
mBmal1	for	5`-ACGACATAGGACACCTCGCAGA-3`

	rev	5`-CGGGTTCATGAAACTGAACCATC-3`
mChop	for	5`-CGAAGAGGAAGAATCAAAAACCTT-3`
	rev	5`-GCCCTGGCTCCTCTGTCA-3`
hCHOP	for	5`- GGAAATGAAGAGGAAGAATCAAAAAT-3`
	rev	5`-GTTCTGGCTCCTCCTCAGTCA-3`
mFas	for	5`-CATTGGTGGTGTGGACATGGT -3`
	rev	5`-GACCGCTTGGGTAATCCATAGA-3`
hFGF21	for	5`-ACCAGAGCCCCGAAAGTCT-3`
	rev	5`-CTTGACTCCCAAGATTTGAATAACTC-3`
mFgfr1c	for	5`-TGTTTGACCGGATCTACACACA-3`
	rev	5`-CTCCCACAAGAGCACTCCAA-3`
mGlut1	for	5`-GCCCCCAGAAGGTTATTGA-3`
	rev	5`-CGTGGTGAGTGTGGTGGAT-3`
hGAPDH	for	5`-GGCCTCCAAGGAGTAAGACC-3`
	rev	5`-AGGGGTCTACATGGCAACTG-3`
mHmgcs2	for	5`-TCTTTTCATTCCGAGTGTCCA-3`
	rev	5`-ATCTGACACACTAGACACCAGTTTCTC-3`
mHsd3b5	for	5`-GCTCTTGGAAACCACAAGGAAC-3`
	rev	5`-GACAATCCTCTGGCCAAGAAAC-3`
mL-cpt1α	for	5`-GCAGAGCACGGCAAAATGA-3`
	rev	5`-GGCTTTCGACCCGAGAAGAC-3`
mMcad	for	5`-TGACGGAGCAGCCAATGA-3`
	rev	5`-ATGGCCGCCACATCAGA-3`
hMCAD	for	5`-CCCAGTGGCTGCAGAATATGAT-3`
	rev	5`-AAACCAAGTTCCCAGGCTCTTC-3`
mMup1	for	5`-CAAAACAGAAAAGGCTGGTGA-3`
	rev	5`-TTGTGCAAACCTTTCCTTGA-3`
mOrp150	for	5`-CACTGCACAGAACGTCATGTTCT-3`
	rev	5`-GGTGACGATGGTGCACACA-3`
mRev-Erb α	for	5`-GGACAACCAGCCCTCAGTTC-3`
	rev	5`-GCAGCTTCGGACCCATGTT-3`
hREV-ERB α	for	5`-ATGACCAAGTCACCCTGCTTAG-3`

	rev	5`-TCTGGTCCTTCACGTTGAACAA-3`
mPparα	for	5`-CAAGGCCTCAGGGTACCACTAC-3`
	rev	5`-GCCGAATAGTTCGCCGAAA-3`
*h*PPARα	for	5`-TGAAGTTCAATGCACTGGAACTG-3`
	rev	5`-GGACGATCTCCACAGCAAATG-3`
mPparβ/δ	for	5`-GCCACAACGCACCCTTTG-3`
	rev	5`-CCACACCAGGCCCTTCTCT-3`
mScd1	for	5`-CTGTACGGGATCATACTGGTTC-3`
	rev	5`-GCCGTGCCTTGTAAGTTCTG-3`

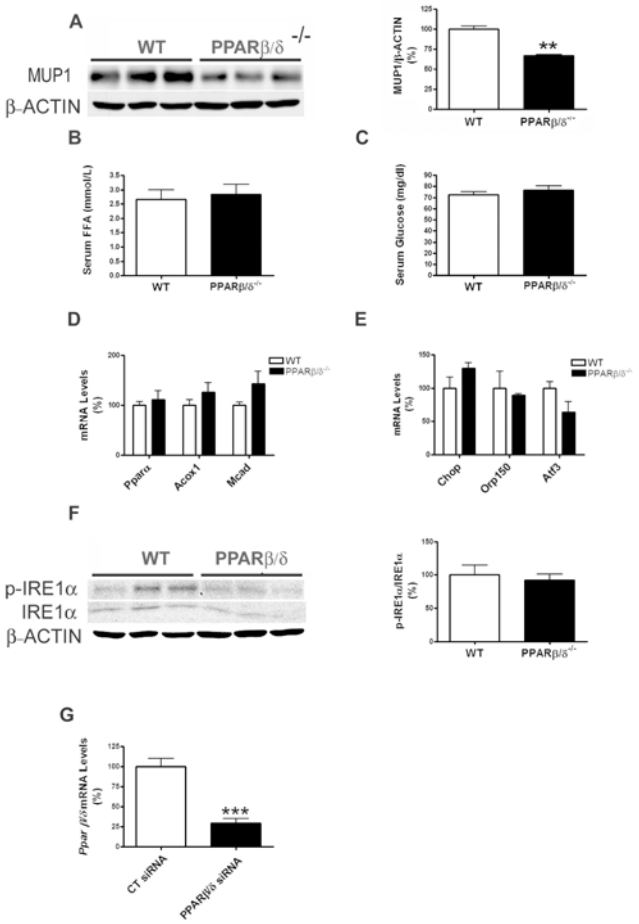

Supplementary Figure 1

209x297mm (300 x 300 DPI)

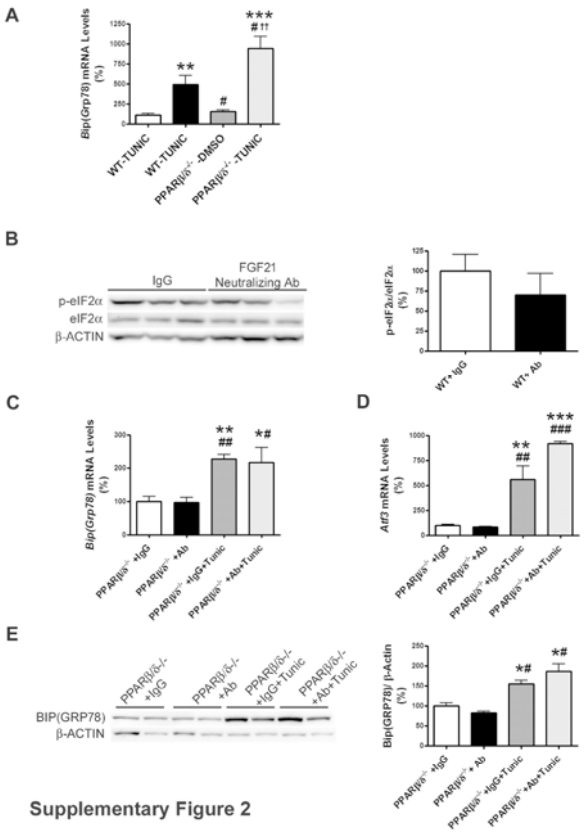

Supplementary Figure 2

209x297mm (300 x 300 DPI)

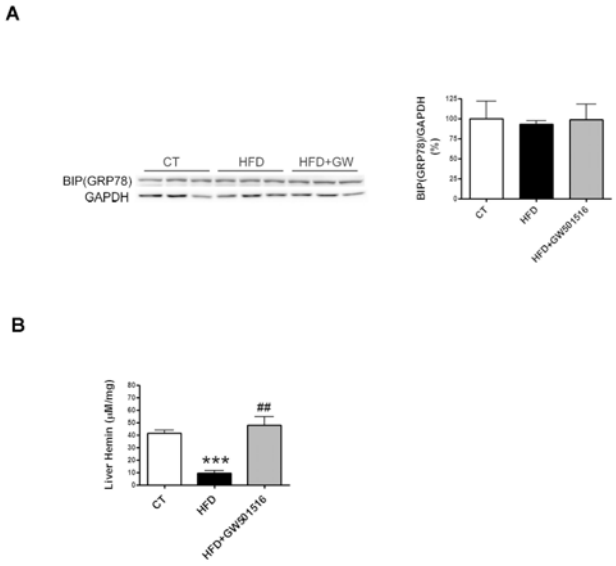

Supplementary Figure 3

209x297mm (300 x 300 DPI)

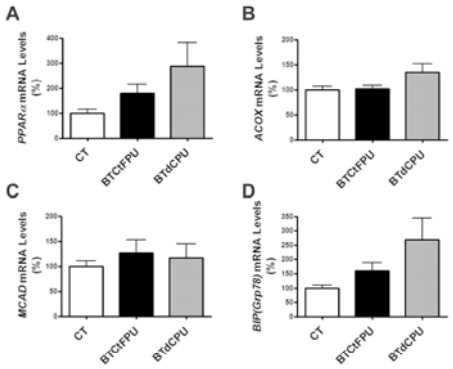

Supplementary Figure 4

209x297mm (300 x 300 DPI)

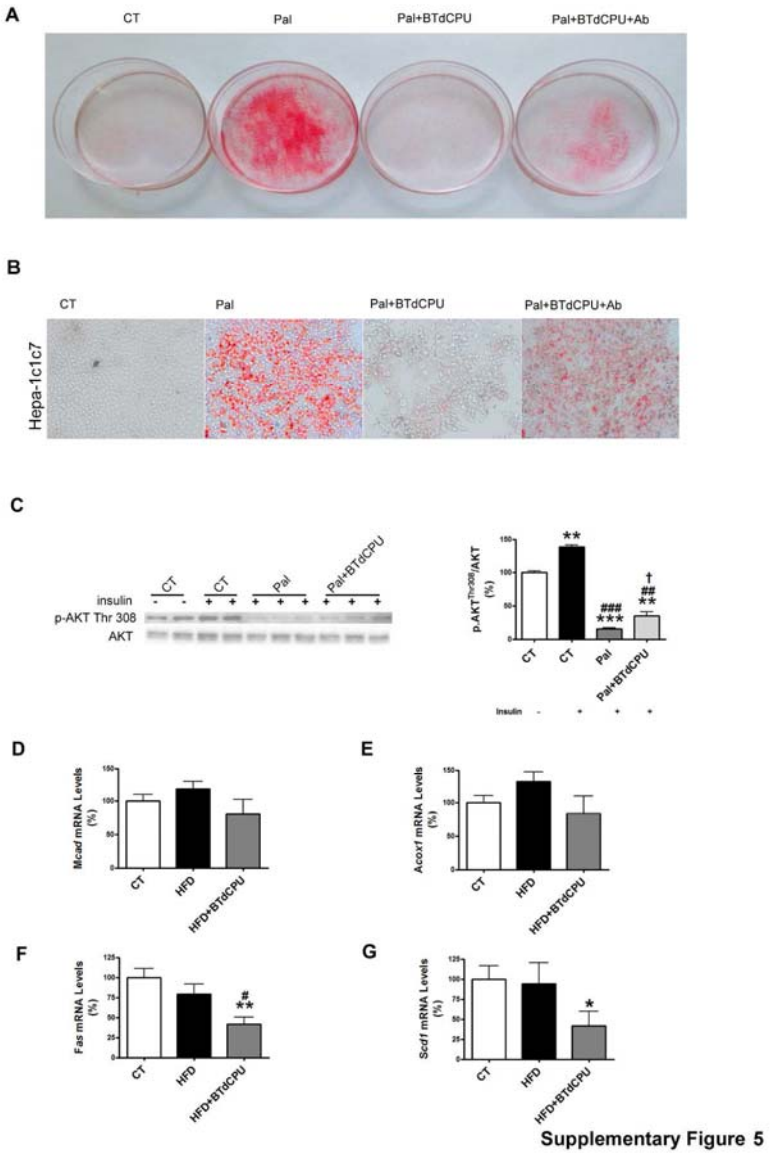

Supplementary Figure 5

209x297mm (300 x 300 DPI)